

# Mechanisms of Native and Artificial Spinning of Spider Silk

Marlene Andersson

*Faculty of Veterinary Medicine and Animal Sciences  
Department of Anatomy, Physiology and Biochemistry  
Uppsala*

Doctoral Thesis  
Swedish University of Agricultural Sciences  
Uppsala 2016

Acta Universitatis agriculturae Sueciae

2016:80

Cover: Photograph of a major ampullate gland from the “Golden orbweaver”

*Nephila clavipes*

(Photo: Marlene Andersson)

ISSN 1652-6880

ISBN (print version) 978-91-576-8662-6

ISBN (electronic version) 978-91-576-8663-3

© 2016 Marlene Andersson, Uppsala

Print: SLU Service/Repro, Uppsala 2016

# Mechanisms of Native and Artificial Spinning of Spider Silk

## Abstract

Spider silk is tougher than all other known natural and man-made fibers, and represents an environmentally friendly material that could potentially be used for many different purposes, ranging from biomaterials to construction materials. However, for large-scale production of silk, methods to produce artificial silk fibers must be developed. In this thesis, the molecular mechanisms of silk spinning were studied with the aim of developing a biomimetic method for production of artificial spider silk fibers.

Major ampullate glands of spiders were studied using light and transmission electron microscopy. Three different epithelial cell types were identified in the tail and sac, two of which produce spider silk proteins (spidroins) that make up the silk and one of which produces carbonic anhydrase that maintains a pH gradient along the gland. The pH gradient was determined to go from pH 7.6 in the tail to pH 5.7 halfway along the duct. Silkworm silk glands were also shown to contain several different epithelial cell types and it was determined that carbonic anhydrase maintains a pH gradient from 8.2 to 6.2 along the gland.

Spidroins consist of a repetitive region with alternating poly-alanine blocks and glycine-rich repeats, flanked by highly conserved globular domains, the N-terminal (NT) and C-terminal (CT) domain. Recombinant versions of NT and CT were studied under the conditions found in the major ampullate gland, and were shown to regulate fiber formation by responding to pH in coordinated but opposite ways, following a lock and trigger mechanism. While NT gets more stable and dimerizes as pH is lowered, and thereby interconnects the spidroins into large networks (lock), CT is destabilized, unfolds and turns into  $\beta$ -sheet amyloid-like fibrils in response to low pH and high  $p\text{CO}_2$ , which may nucleate further  $\beta$ -sheet formation of the repetitive region (trigger).

Based on the knowledge generated on native silk spinning, a biomimetic method to spin artificial spider silk fibers was developed. A chimeric recombinant spidroin was designed by combining a highly soluble NT and CT with a short repetitive region. The extremely soluble spidroin could be concentrated to unprecedented levels, and formed tough, kilometer-long fibers upon spinning into a low pH aqueous buffer.

*Keywords:* major ampullate gland, spidroin, silkwork, carbonic anhydrase, pH, major, biomimetic, spinning, fiber, protein structure and function

*Author's address:* Marlene Andersson, SLU, Department of Anatomy, Physiology and Biochemistry, P.O. Box 7011, 750 07 Uppsala Sweden

*E-mail:* marlene.andersson@slu.se

To my family

*Look deep into Nature, and then you will understand everything better.*

Albert Einstein

# Contents

List of Publications	7
Abbreviations	9
<b>1 Introduction</b>	<b>11</b>
1.1 Spider silk	12
1.1.1 The major ampullate gland	12
1.1.2 Dragline silk	14
1.1.3 Silk formation in the major ampullate gland	14
1.1.4 Major ampullate spidroins	15
1.1.5 Additional silk types and their corresponding spidroins	22
1.1.6 Mechanical properties of native spider silks	22
1.2 Silkworm silk	24
1.2.1 Silkworm silk glands	24
1.2.2 Silk formation in <i>Bombyx mori</i>	25
1.2.3 Fibroins	26
1.2.4 Mechanical properties of native silkworm silk	27
1.3 Artificial spider silk	27
1.3.1 Recombinant spidroins: purification and spinning	27
1.3.2 Mechanical properties of artificial fibers	32
1.4 Carbonic anhydrase	33
1.5 Amyloid	33
<b>2 Present investigation</b>	<b>35</b>
2.1 Aims of this thesis	35
2.2 Materials and methods	35
2.2.1 Histochemical localization of carbonic anhydrase activity	36
2.2.2 Determination of ion concentrations in silk glands	36
2.2.3 Studies of recombinant NT and CT	38
2.2.4 Tensile tests of artificial spider silk fibers	41
2.3 Results	42
2.3.1 Paper I: Morphology and composition of the major ampullate gland and dragline silk	42
2.3.2 Paper II: Carbonic anhydrase generates CO <sub>2</sub> and H <sup>+</sup> that drive spider silk formation via opposite effects on the terminal domains	43
2.3.3 Paper III: Carbonic anhydrase generates a pH gradient in <i>Bombyx mori</i> silk glands	46

2.3.4	Paper IV: Biomimetic spinning of artificial spider silk from an extremely concentrated chimeric minispidroin	47
2.4	Discussion	49
<b>3</b>	<b>Conclusions and outlook</b>	<b>55</b>
<b>4</b>	<b>Populärvetenskaplig sammanfattning</b>	<b>57</b>
	<b>References</b>	<b>59</b>
	<b>Acknowledgements</b>	<b>71</b>

## List of Publications

This thesis is based on the work contained in the following papers, referred to by Roman numerals in the text:

- I **Andersson M**, Holm L, Ridderstråle Y, Johansson J, Rising A. (2013) Morphology and composition of the major ampullate gland and dragline silk. *Biomacromolecules* 14, 2945-2952.
- II **Andersson M\***, Chen G\*, Otikovs M, Landreh M, Nordling K, Westermark P, Jörnvall H, Knight SD, Ridderstråle Y, Holm L, Meng Q, Jaudzems K, Chesler M, Johansson J, Rising A. (2014) Carbonic anhydrase generates CO<sub>2</sub> and H<sup>+</sup> that drive spider silk formation via opposite effects on the terminal domains. *PLoS Biol* 12, 1-14. \*These authors contributed equally to this work.
- III Domigan LJ\*, **Andersson M\***, Alberti KA, Chesler M, Xu, Q, Johansson J, Rising A, Kaplan DL. (2015) Carbonic anhydrase generates a pH gradient in *Bombyx mori* silk glands. *Insect Biochem Mol Biol* 65, 100-106. \*These authors contributed equally to this work.
- IV **Andersson M\***, Jia Q\*, Abella A, Lee XY, Landreh M, Purhonen P, Hebert H, Tenje M, Robinson CV, Meng Q, Plaza G, Johansson J, Rising A. (2016) Biomimetic spinning of artificial spider silk from an extremely concentrated chimeric minispidroin. Manuscript. \*These authors contributed equally to this work.

Papers I-III are reproduced with the kind permission of the publishers.

Papers not included in the thesis:

Kronqvist N, Otkovs M, Chmyrov V, Chen G, **Andersson M**, Nordling K, Landreh M, Sarr M, Jörnvall H, Wennmalm S, Widengren J, Meng Q, Rising A, Otzen D, Knight SD, Jaudzems K, Johansson J. (2014) Sequential pH-driven dimerization and stabilization of the N-terminal domain enables rapid spider silk formation. *Nat Commun*, 5:3254. DOI: 10.1038/ncomms4254

**Andersson M**, Johansson J, Rising A. (2016) Review: Silk spinning in silkworms and spiders. *Int J Mol Sci*, 17:1290. DOI: 10.3390/ijms17081290

## Abbreviations

ASG	Anterior silk gland
CA	Carbonic anhydrase
CD	Circular dichroism
CT	C-terminal domain
ESI-MS	Electrospray ionization
FibCT	C-terminal segment of the fibroin heavy chain
FibNT	N-terminal domain of the fibroin heavy chain
Fibroin	Silkworm silk protein
FTIR	Fourier transform infrared spectroscopy
HDX	Hydrogen-deuterium exchange
HFIP	Hexafluoroisopropanol
IMAC	Immobilized metal ion affinity chromatography
ISM	Ion-selective microelectrode
LC-MS	Liquid chromatography mass spectroscopy
LM	Light microscopy
MaSp	Major ampullate spidroin
Minispidroin	Miniature spider silk protein (recombinant)
MiSp	Minor ampullate spidroin
MS	Mass spectroscopy
MSG	Middle silk gland
NMR	Nuclear magnetic resonance
NT	N-terminal domain
PSG	Posterior silk gland
Spidroin	Spider silk protein
TEM	Transmission electron microscopy
ThT	Thioflavin T

One letter codes for the 20 naturally occurring amino acids.

Alanine	A
Arginine	R
Asparagine	N
Aspartic acid	D
Cysteine	C
Glutamic acid	E
Glutamine	Q
Glycine	G
Histidine	H
Isoleucine	I
Leucine	L
Lysine	K
Methionine	M
Phenylalanine	F
Proline	P
Serine	S
Threonine	T
Tryptophan	W
Tyrosine	Y
Valine	V

# 1 Introduction

Spiders and silkworms spin silk fibers with remarkable properties. Not only are they exceptionally tough (Omenetto & Kaplan, 2010), but spider silk fibers are also well tolerated when implanted in living tissues (Vollrath *et al.*, 2002; Allmeling *et al.*, 2008; Radtke *et al.*, 2011). Furthermore, native silks represent an environmentally friendly material since they are produced from renewable sources at ambient temperatures. Thus, silk is an attractive material for many different areas, ranging from regenerative medicine to the construction industry. The amazing properties of silk were discussed already in the beginning of the 18<sup>th</sup> century, when it was suggested that spider silk could be used to stop bleeding (Bon, 1710).

Silkworms are easy to house and produce large amounts of silk that is used as a suture material and in the textile industry. However, biomedical applications of silkworm silk require removal of sericin (a protein that coats the silk fiber) that may otherwise cause an allergic response (Altman *et al.*, 2003). In contrast, spider silk fibers do not contain sericin and may be a better biomaterial, but spiders are difficult to house and produce small amounts of silk (Winkler & Kaplan, 2000). Thus, successful large-scale production of spider silk fibers requires expression and purification of silk proteins from heterologous hosts, followed by spinning into fibers.

Despite significant efforts to produce artificial spider silk, the outstanding mechanical properties of native silk have not yet been possible to mimic, partly as a result of poor understanding of native silk production mechanisms. In this thesis, the silk glands and molecular mechanisms of silk spinning were studied in silkworms and spiders in order to develop a biomimetic method for production of artificial spider silk.

## 1.1 Spider silk

Spiders spin their silk from spider silk proteins (spidroins) that are produced in abdominal glands. There are several different types of glands, each responsible for producing a specific type of silk with unique mechanical properties. Some spiders have up to seven different glands, including the major ampullate, minor ampullate, flagelliform, aggregate, pyriform, tubuliform (also referred to as cylindriform), and aciniform glands (Figure 1) (Peakall, 1969). The histology of these glands was studied thoroughly during the 1980s and 1990s (Kovoor, 1987; Kovoor, 1990; Tillinghast, 1994). Since then, most studies (including this thesis) have been focused on the major ampullate gland (Vollrath & Knight, 1999; Casem *et al.*, 2002; Davies *et al.*, 2013).

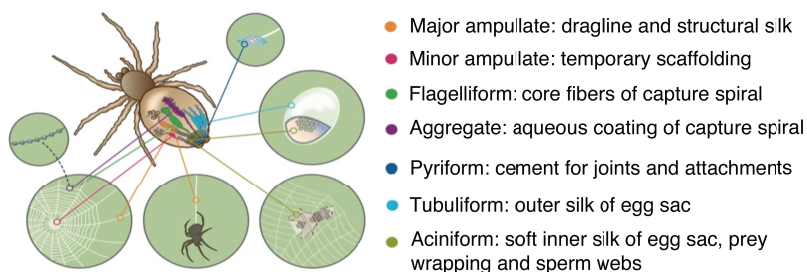


Figure 1. Illustration of the seven silk glands present in a female orbweaver and their respective primary use. Adapted with permission from Macmillan Publishers Ltd: *Nature Chemical Biology*, (Rising & Johansson), copyright (2015).

Spidroins are stored in the gland as a concentrated aqueous solution, called the spinning dope (Hijirida *et al.*, 1996; Chen *et al.*, 2002). Upon spinning, the dope travels through the gland and experiences changes in the microenvironment that cause the spidroins to go from a soluble state to a solid fiber in fractions of a second. Spidroins share an overall architecture with two highly conserved hydrophilic terminal domains, the N-terminal (NT) (Rising *et al.*, 2006) and C-terminal (CT) domain (Garb *et al.*, 2010), flanking a large and repetitive region (Ayoub *et al.*, 2007). The NT and CT are likely contributing to the extreme solubility of native spidroins in the spinning dope of spiders (Askarieh *et al.*, 2010; Hagn *et al.*, 2010), while the repetitive region confers the mechanical properties to the silk fiber (Hayashi *et al.*, 1999).

### 1.1.1 The major ampullate gland

The paired major ampullate gland can be divided into three distinct parts: a tail, a sac, and an s-shaped duct (Bell & Peakall, 1969) (Figure 2). Spidroins are produced in the tail and proximal part of the sac, and are secreted into the lumen where they are stored. The dope then flows through the duct that leads

to the spinneret where the fiber is pulled out by the spider's leg or by other means such as gravity, wind, or movement of the spider in the web (Vollrath & Knight, 2001).

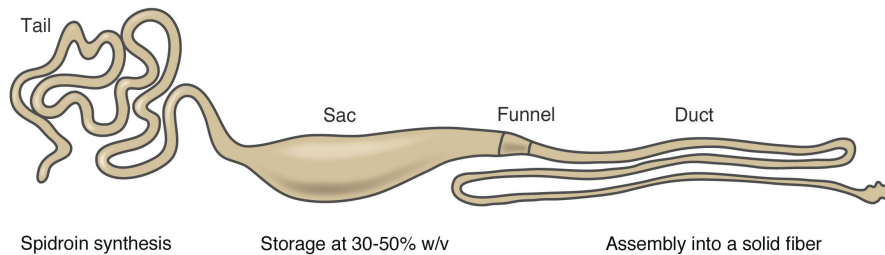


Figure 2. The major ampullate gland consists of a long tail where spidroins are produced, a sac where they are stored, and a duct along which the spidroins are assembled into a solid fiber. The sac and duct are connected to each other by the funnel. Adapted with permission from Elsevier: *Acta Biomaterialia* (Rising), copyright (2014).

Both the tail and sac consist of a single layer of columnar epithelial cells (Kovoor, 1987). The spidroin expression capacity is high in the tail and proximal part of the sac, as indicated by the abundant rough endoplasmic reticulum and the large number of secretory granules within the cells (Bell & Peakall, 1969; Casem *et al.*, 2002). Early on, a few studies reported the presence of three different cell types in major ampullate glands, but their respective functions were not examined (Kovoor, 1987; Kovoor, 1990; Tillinghast, 1994). Since then, the common opinion has been that there are two different epithelial cell types in the major ampullate tail and sac, referred to as the A and B zones (Knight & Vollrath, 1999; Knight & Vollrath, 2001; Dicko *et al.*, 2004; Sponner *et al.*, 2007). The A zone is responsible for expression and secretion of spidroins (Sponner *et al.*, 2004), while the B zone produces either non-spidroin components such as lipids and carbohydrates or another type of spidroin (Vollrath & Knight, 2001; Sponner *et al.*, 2007).

The funnel connects the sac to the duct (Figure 2) (Bell & Peakall, 1969), but the functions of the funnel have not been determined. The duct is folded into an s-shape, ending in a spigot on the anterior spinneret (Bell & Peakall, 1969; Kovoor, 1987). A single epithelial cell layer with microvilli at the apical cell membrane lines the duct, which suggests that the duct is involved in dehydration of the spidroins upon spinning (Casem *et al.*, 2002). There is a layer between the lumen and the apical cell membrane referred to as the cuticular intima, which is hypothesized to protect the underlying cells during fiber formation (Davies *et al.*, 2013). The cuticular intima has also been proposed to act as a dialysis membrane allowing for dehydration of the

spinning dope (Vollrath & Knight, 1999). The diameter of the duct lumen is progressively narrowing, and goes from around 100  $\mu\text{m}$  to  $<10 \mu\text{m}$  (Knight & Vollrath, 1999; Davies *et al.*, 2013).

### 1.1.2 Dragline silk

The major ampullate gland is the source of dragline silk, which is made up of at least two different major ampullate spidroins (MaSp), MaSp 1 and 2 (Hinman & Lewis, 1992; Ayoub *et al.*, 2007). Dragline silk fibers are 1-6  $\mu\text{m}$  in diameter (Perez-Rigueiro *et al.*, 2001; Sampath *et al.*, 2012; Xu *et al.*, 2015) and have a core-skin architecture with spidroins in the core and carbohydrates, lipids or non-spidroin proteins in the skin. The skin and core have, in some studies, been further divided in up to five layers but the composition and number of these layers have been debated (Li *et al.*, 1994; Vollrath *et al.*, 1996; Frische *et al.*, 1998; Augsten *et al.*, 2000; Sponner *et al.*, 2007). Studies on fiber architecture have involved extensive treatment such as dehydration, embedding in plastic, sectioning and staining (Frische *et al.*, 1998; Augsten *et al.*, 2000), dipping silk fibers in urea (Vollrath *et al.*, 1996) or treating fibers using ether, triton x-100 and freeze-thaw cycles (Sponner *et al.*, 2007), which makes it difficult to draw conclusions about the native structure of dragline silk. While some studies have not identified subfibrillar structures in the fiber (Thiel *et al.*, 1994; Thiel *et al.*, 1997), others show that the core is composed of micro- and nanofibrils parallel to the fiber axis which may contribute to the mechanical properties of dragline silk (Li *et al.*, 1994; Vollrath *et al.*, 1996; Gould *et al.*, 1999; Miller *et al.*, 1999; Augsten *et al.*, 2000; Sponner *et al.*, 2007).

The localization and distribution of MaSp 1 and 2 in the fiber was studied by Sponner and coauthors, using antibodies directed against the MaSp 1 or 2 repetitive region (Sponner *et al.*, 2005a; Sponner *et al.*, 2005b; Sponner *et al.*, 2007). They concluded that MaSp1 is more abundant in the dragline silk fiber than MaSp2 and that MaSp1 is present throughout the core region of the fiber but not in the skin layers, while MaSp2 is present only in certain areas in the inner core of the fiber (Sponner *et al.*, 2005a; Sponner *et al.*, 2005b). It was further shown that CT is present in the core but not in the skin of the fiber (Sponner *et al.*, 2004). The distribution of NT has not been studied in major ampullate glands or in dragline silk.

### 1.1.3 Silk formation in the major ampullate gland

Major ampullate spidroins are stored in a soluble state at 30-50% w/v, *i.e.* 300-500 mg/ml in the sac (Figure 2) (Hijirida *et al.*, 1996; Chen *et al.*, 2002). A long-standing question has been how the spider manages to keep the proteins

in solution at such high concentrations, yet rapidly turns them into a solid fiber at the spinneret. The high solubility of spidroins could in part be mediated by the spidroins forming micelles where hydrophobic regions are shielded in the core, while hydrophilic regions such as the terminal domains form the outer shell (Lin *et al.*, 2009). The micelles are suggested to elongate and fuse in response to increased shear forces and lowered pH (Eisoldt *et al.*, 2011). The spidroins have also been suggested to be stored as a liquid crystalline feedstock (Kerkam *et al.*, 1991; Willcox & Gido, 1996; Knight & Vollrath, 1999), meaning that the spidroins order in a regular manner as in a crystal, but flow like a liquid. This allows the dope to flow through the sac and the first limb of the duct before forming a fiber at the end of the duct (Knight & Vollrath, 1999; Vollrath & Knight, 2001). The two models are not mutually exclusive, and further experimental studies are warranted to fully elucidate the storage mechanism of the spinning dope in the gland.

A combination of several factors such as lowered pH, shear forces and ion exchange alters the conformation of spidroins, causing them to go from a soluble spinning dope to a solid fiber. A pH gradient going from 6.9 in the sac to around 6.3 in the end of the duct (Knight & Vollrath, 2001) or from 7.2 in the sac to 6.3 in the funnel (Dicko *et al.*, 2004) has been determined. The generation of a pH gradient has been attributed to the presence of ATPase-driven proton pumps along the duct. Inhibition of these pumps results in halted acidification in the duct, indicating that they are vital for the pH gradient (Vollrath *et al.*, 1998).

As the spinning dope flows through the duct, it eventually pulls away from the walls of the duct, and forms a solid fiber through a pH- and shear-induced phase transition (Knight & Vollrath, 1999; Knight *et al.*, 2000). The phase-transition is likely due to a structural conversion into  $\beta$ -sheets of the spidroins in response to shear forces (Giesa *et al.*, 2016) and pH. The spinning dope is dehydrated along the duct (Vollrath & Knight, 1999; Casem *et al.*, 2002). The water uptake by the epithelial cells in the duct may be associated with sodium and chloride reabsorption since levels of sodium and chloride in the lumen decrease along the duct, while potassium, phosphorus and sulphur levels increase (Knight & Vollrath, 2001).

#### 1.1.4 Major ampullate spidroins

Although dragline silk is considered to be composed mainly of MaSp1 and 2 (Hinman & Lewis, 1992; Ayoub *et al.*, 2007), recent whole genome sequencing of a velvet spider (*Stegodyphus mimosarum*) identified up to ten putative MaSp genes. In addition, more than 100 other, non-spidroin proteins have been identified in the dragline silk fiber (Sanggaard *et al.*, 2014). Since

the proteins that are encoded by these putative genes have not been characterized, the focus herein will be on the relatively well characterized MaSp1 and 2. They both consist of an NT (Rising *et al.*, 2006), a CT (Hagn *et al.*, 2010), and a large repetitive region (Ayoub *et al.*, 2007) (Figure 3).

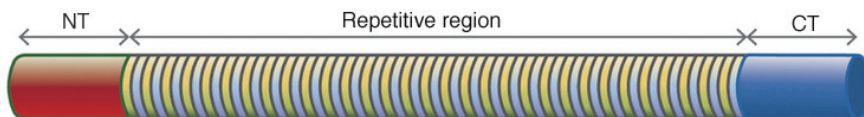


Figure 3. Schematic illustration of a MaSp consisting of an N-terminal domain (NT), a repetitive region and a C-terminal domain (CT). Adapted with permission from Macmillan Publishers Ltd: *Nature Chemical Biology*, (Rising & Johansson), copyright (2015).

### *The N-terminal domain*

The NT is around 130 amino acid residues long and is evolutionary conserved both between spider silk types and spider species (Rising *et al.*, 2006). It folds into a five-helix bundle monomer with a dipolar charge distribution at neutral pH (Askarieh *et al.*, 2010; Gaines *et al.*, 2010; Hagn *et al.*, 2011; Jaudzems *et al.*, 2012; Kronqvist *et al.*, 2014). Upon a lowering of pH, NT assembles into an antiparallel dimer, thereby interconnecting the spidroins (Hedhammar *et al.*, 2008; Askarieh *et al.*, 2010; Gaines *et al.*, 2010; Hagn *et al.*, 2011; Schwarze *et al.*, 2013; Otikovs *et al.*, 2015; Atkison *et al.*, 2016). The structural rearrangements that are required for the interconversion from monomer to dimer include relocation of the only tryptophan residue present in MaSp1 NT, which allows for repositioning of helix 3, thereby leading to formation of the dimer interface (Askarieh *et al.*, 2010; Gaines *et al.*, 2010; Jaudzems *et al.*, 2012; Atkison *et al.*, 2016). The tryptophan sidechain goes from being buried in the center of the helix bundle in the monomer to a more solvent-exposed location in the dimer (Figure 4), thereby offering the possibility to use tryptophan fluorescence spectroscopy to follow the monomer to dimer conversion (Gaines *et al.*, 2010; Jaudzems *et al.*, 2012). The ratio between the fluorescence at 339 and 351 nm at a specific pH represents the ratio between monomeric and dimeric NT (Kronqvist *et al.*, 2014).

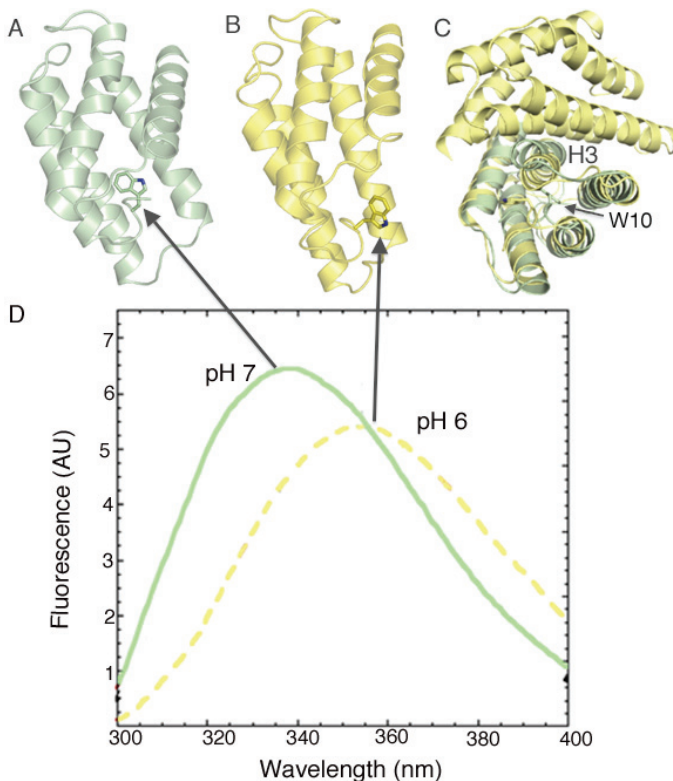


Figure 4. (A) The tryptophan side chain is buried in the core of the protein in the N-terminal monomer. (B) In a subunit of the N-terminal dimer, the tryptophan side chain is more solvent exposed. (C) Helix 3 (H3) is relocated in the dimer structure, as seen by superimposing the nuclear magnetic resonance (NMR) structure of the N-terminal monomer (pale green) and crystal structure of the N-terminal dimer (yellow). (D) Upon going from pH 7 to pH 6, NT dimerizes, the tryptophan side chain changes its location and a red-shift in emission occurs. AU: arbitrary units. Arrows point to the tryptophan side-chain. W10: tryptophan residue 10. Crystal and NMR structures determined in (Askarieh *et al.*, 2010; Jaudzems *et al.*, 2012).

According to tryptophan fluorescence spectroscopy, NT dimerization is completed around pH 6 (black curve in Figure 5). Stability studies by urea denaturation show that full NT stabilization occurs after dimerization is completed, as NT continues to stabilize all the way down to pH 5 (blue curve in Figure 5).

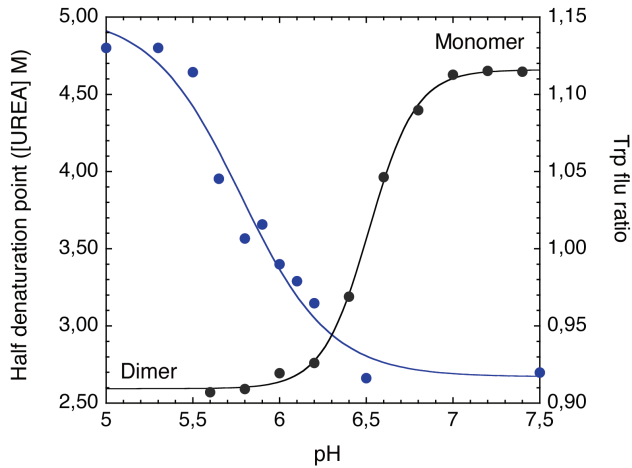


Figure 5. Dimerization and stabilization of the N-terminal domain (NT) are decoupled events as illustrated by plotting half denaturation point in molar urea (blue, left axis) and the ratio of tryptophan fluorescence between 339 and 351 nm (black, right axis) against pH. High tryptophan fluorescence (Trp flu) ratio indicates presence of NT monomers, while low flu ratio indicates presence of NT dimers. Data from Kronqvist *et al.*, (2014).

Detailed analysis of the dimerization and stabilization of recombinant MaSp1 NT from *Euprosthenoops australis* led to the description of a three step mechanism (Figure 6) (Kronqvist *et al.*, 2014). The NT monomer subunits are weakly associated at neutral pH due to electrostatic interactions between amino acid residues D40, K65 and R60 (and possibly E84). Next, at around pH 6.5 residues E79 and E119 are becoming protonated. This leads to association and pre-alignment of the subunits and subsequently to formation of loosely connected dimers in which the structural rearrangements of the tryptophan residue side-chain and helix 3 occur (measured by tryptophan fluorescence spectroscopy, Figure 5). This state still permits movements of NT subunits in respect to each other (Kronqvist *et al.*, 2014; Atkison *et al.*, 2016). The weakly associated dimers may have a dual role: (i) to permit structural rearrangements of the spidroins which may protect against retrograde propagation of the pulling forces, and (ii) to enable stable NT dimers to form very rapidly, since it would be independent of diffusion rate. When pH drops to 5.7 or below, E84 is becoming protonated thereby allowing the formation of a fully stable dimer (measured by urea stability studies, Figure 5) (Kronqvist *et al.*, 2014). Stable dimerization of NT interconnects the spidroins, which may allow the pulling forces in the fiber to be propagated via the protein chains, thereby facilitating the structural conversion of the repetitive parts.

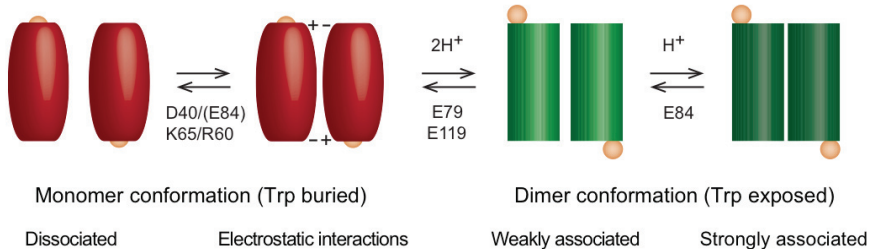


Figure 6. At high pH, NT is present in monomer conformation. Electrostatic interactions mediated by D40, K65, R60 and possibly E84 lead to a weak association of NT monomer subunits. Around pH 6.5, E79 and E119 are protonated, leading to the formation of a weakly associated dimer conformation in which the tryptophan side chain (Trp) becomes exposed to a more polar environment. Finally, at around pH 5.7, strongly associated and fully stable NT dimers are formed when E84 is protonated. Reproduced with permission from Macmillan Publishers Ltd: *Nature Communications*, (Kronqvist *et al.*) copyright (2014).

### *The C-terminal domain*

The CT is around 110 amino acid residues long (Chen *et al.*, 2012) and folds into a five-helix bundle, but with a different topology than NT. It is a constitutive parallel dimer stabilized via a disulfide bond in the case of MaSpS (Hagn *et al.*, 2010) or held together only by hydrophobic and other non-covalent interactions as in minor ampullate spidroin (MiSp) CTs (Gao *et al.*, 2013). The CT is conserved between spidroin types, but to a lesser extent than NT (Chen *et al.*, 2012). For example, a conserved salt bridge between an arginine residue (helix 2) and a glutamic acid residue (helix 4) has been identified in CT. Shear forces and high salt conditions causes CT to unfold and aggregate (Hagn *et al.*, 2010; Gao *et al.*, 2013), but it is essentially pH insensitive down to pH 6 (Askarieh *et al.*, 2010; Hagn *et al.*, 2010). Recombinant spidroins that include CT form well-defined fibrous aggregates, while spidroins expressed without CT are prone to unspecific aggregation (Ittah *et al.*, 2006; Hedhammar *et al.*, 2008; Hagn *et al.*, 2010).

### *The repetitive region*

The MaSp repetitive region can be up to 3000 amino acid residues long and contains up to 100 ensemble repeats with alternating motifs of poly-alanine blocks (4-12 amino acid residues) and glycine-rich repeats of different lengths (Table 1) (Ayoub *et al.*, 2007). The glycine-rich repeats of MaSp2 contain prolines, but is otherwise similar to MaSp1 (Hinman & Lewis, 1992).

### *Secondary structures of major ampullate spidroins in solution and fiber*

Numerous studies have determined the secondary structure of MaSps in the dope (*i.e.* in solution), by studying native spinning dopes using nuclear magnetic resonance (NMR), Fourier transform infrared spectroscopy (FTIR), circular dichroism (CD), and Raman spectroscopy. Although it has been difficult to conclusively assign structures, soluble MaSps have been shown to contain mostly random coils,  $\alpha$ -helices and helices with three amino acid residues per turn (referred to in the table and the text from now on as  $3_1$  helices) (Hijirida *et al.*, 1996; Hronska *et al.*, 2004; Lawrence *et al.*, 2004; Lefevre *et al.*, 2008; Lefevre *et al.*, 2011a; Lefevre *et al.*, 2011b).

The MaSps changes into  $\beta$ -sheet fibrils at the end of the duct, as demonstrated by CD spectroscopy, transmission electron microscopy (TEM) and Congo red staining (Knight *et al.*, 2000; Kenney *et al.*, 2002; Dicko *et al.*, 2004; Plaza *et al.*, 2006). The dragline silk fiber is composed of highly organized  $\beta$ -sheets embedded in an amorphous matrix (that despite its name contains ordered secondary structures). X-ray diffraction and solid state NMR show that the  $\beta$ -strands are oriented parallel to the fiber axis and that  $\beta$ -sheets make up 35-40% of the fiber (Table 1). The  $\beta$ -sheets are dominated by poly-alanine blocks (van Beek *et al.*, 2002; Jenkins *et al.*, 2010; Jenkins *et al.*, 2013; Xu *et al.*, 2015). The amorphous region is partially oriented, contains  $\beta$ -turns and  $3_1$  helices, and is composed mainly of glycine residues (van Beek *et al.*, 2002; Holland *et al.*, 2008; Jenkins *et al.*, 2013; Xu *et al.*, 2015).

Table 1. The different silk types are composed of spidroins that have specific ensemble repeats within their repetitive regions. The individual motifs of these ensemble repeats fold into different secondary structures in the fiber. Only the spidroins that form fibers are included herein

Silk type	Overall spidroin architecture	Ensemble repeat (R)	Residue motifs	Main secondary structures in the fiber	References
Dragline	NT-(R) <sub>100</sub> -CT	MaSp1: GQGQGGYGGGLGGGYGGAGSSAAAAA	Poly-A, (GA) <sub>n</sub>	β-sheet, 35-40%	1-7
	R size: 25-40 aa residues		GGX	3 <sub>1</sub> helix	
Minor ampullate	NT-(R) <sub>10</sub> -S-(R) <sub>10</sub> -CT	MaSp2: GGAGPGRQQYGGAGAAAAA	Poly-A, (GA) <sub>n</sub>	β-sheet, 35-40%	1-7
	R size: 30-70 aa residues S size: 125-140 aa residues		GGX	3 <sub>1</sub> helix	
Aciniform	NT-(R) <sub>14</sub> -CT	GGXGGY(GX) <sub>4+13</sub> (A) <sub>3+5</sub> (GX) <sub>0+3</sub> GGAGYGGGX(GX) <sub>1-10</sub>	(GA) <sub>n</sub> , poly-A	β-sheet, 35-37%	6, 8-10
	R size: 200 aa residues		GGX	3 <sub>1</sub> helix	
Flagelliform	NT-(R-S) <sub>4</sub> -CT	GSAGPQGGFATGGASAGLISRVANALANTSLRTLVLRTGVSSQQIAS SVVQRAAQSLASITLGDGNNLRFVAQAVSRIPAGSDTSAAYAQAFS SALFNAGVLNASNIDTLGSRVLSALLNGVSSAAQGLGIVDGSVQSS DISSSSFLTSSSSASYSQASASSTSGAGYTGPSGFTGPSYGPPLG GGAPFGQSGFG	Spacer	α-helix	6, 10-11
	R size: 440 aa residues S size: 9-27 aa residues		Poly-S, otherwise low content of specific motifs	β-sheet 30%, 3 <sub>1</sub> helix, α-helix 24%, β-turn	
Tubuliform	NT-(R) <sub>20</sub> -R2-CT	(GPGGX) <sub>0-65</sub> (GGX) <sub>7-12</sub> THIEDLITIDGADGAPITISEELTISGAGGS	GPGXX	β-turn	9, 12, 13
	R size: 170-200 aa residues		GGX	3 <sub>1</sub> helix	
Tubuliform	NT-(R) <sub>20</sub> -R2-CT	TTTTTAGSQAAQSASASASQASASFSARASSASLAASSFSAFSS ANLSALGNVGYQLGFVNANNLGGNAAGLGNALSQAVSSVGVGA SSSTYANAVSNVAGFLAGQGLNNAANAGLSLASSFASALSASAAVA SSAAAQAAASQSQAAASAFSRAASQASASQASARSQAQSSS	Spacer	β-sheet (predicted)	6, 10, 14
	R size: 170-200 aa residues		(S) <sub>n</sub> , (T) <sub>n</sub> , (SX) <sub>n</sub> , otherwise low content of specific motifs	β-sheet 35-37%, 3 <sub>1</sub> helix, α-helix, β-turn	

R: ensemble repeat, S: spacer, NT: N-terminal domain, CT: C-terminal domain, aa: amino acid, X: variable amino acid residue. Amino acid residues are given in one-letter code. (1) Hinman & Lewis (1992), (2) Hayashi *et al.* (1999), (3) Ayoub *et al.* (2007), (4) Jenkins *et al.* (2013) (5) Dicko *et al.* (2004), (6) Lefèvre *et al.* (2011b) (7) van Beek *et al.* (2002), (8) Chen *et al.* (2012), (9) Zhou *et al.* (2001b), (10) Rousseau *et al.* (2009), (11) Hayashi *et al.* (2004), (12) Hayashi *et al.* (1998), (13) Ohgo *et al.* (2006), (14) Tian & Lewis (2006).

### 1.1.5 Additional silk types and their corresponding spidroins

The spidroins discussed herein have an overall architecture with an NT, a CT and a repetitive region which contains ensemble repeats that are specific and characteristic for each spider silk type (Table 1). The MiSps also contain two identical non-repetitive spacer regions, and the ensemble repeat of flagelliform spidroins includes small negatively charged spacer regions that separate the iterated glycine motifs (Hayashi *et al.*, 1999; Chen *et al.*, 2012; Lefevre & Pezolet, 2012; Adrianos *et al.*, 2013).

The MiSps are quite similar to MaSps in terms of secondary structure, both in solution and in fibers. In contrast to MaSps and MiSps, poly-alanine blocks are not common in aciniform, flagelliform or tubuliform spidroins (Hayashi *et al.*, 2004). Instead, aciniform and tubuliform spidroins contain poly-serine blocks and glycine-rich repeats while flagelliform spidroins contain glycine-rich repeats with and without proline (Table 1). The percentage of  $\beta$ -sheet is somewhat lower in aciniform silk than in dragline, minor ampullate and tubuliform silk, but  $\beta$ -sheet is still the dominating structure, closely followed by  $\alpha$ -helices (Table 1) (Rousseau *et al.*, 2009). The  $\beta$ -sheet content in flagelliform silk is very low, but there is a high  $\beta$ -turn content that likely leads to formation of  $\beta$ -spirals (Hayashi *et al.*, 1999; Ohgo *et al.*, 2006).

Despite having very different amino acid residue composition of their ensemble repeats, the different spider silk types contain the same types of secondary structure elements, but there is a difference in the relative amount of each element, which probably influences mechanical properties, as discussed below.

### 1.1.6 Mechanical properties of native spider silks

Spider silks are the toughest fibers known to man, outcompeting all known natural and manmade fibers, including for example tendons, silkworm silk, rubber, nylon, steel and Kevlar (Gosline *et al.*, 1999; Omenetto & Kaplan, 2010). Stress-strain curves can be used to study the tensile behavior of a silk fiber. The stress (*i.e.* strength of the fiber) is calculated from the force that the fiber can withstand divided by the initial cross-sectional area of the fiber, while strain is a measure of the extensibility of the fiber. The maximum stress before breaking of the fiber is referred to as the ultimate tensile strength, and the stiffness is referred to as elastic modulus. The elastic modulus can be calculated from the slope of the initial part of the stress/strain curve (during elastic deformation, before the yielding point, Figure 7). Toughness is a measure of how much energy is required to break a fiber and is equal to the area under the stress-strain curve, shaded in Figure 7. All spider silk types described herein, except flagelliform silk, display an initial elastic deformation

up to a yielding point, after which plastic deformation occurs until rupture (Figure 8) (Blackledge & Hayashi, 2006). Elastic deformation is a reversible deformation that occurs when a material is subjected to minor stress, while higher stresses lead to plastic deformation, which is irreversible (Hosford *et al.*, 2004). Although Kevlar and high-tensile steel have higher ultimate tensile strength and stiffness than spider silk, they do not reach the same toughness since they are not nearly as extendible (Gosline *et al.*, 1999; Omenetto & Kaplan, 2010).

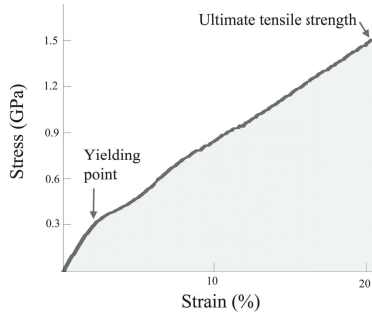


Figure 7. Representative stress/strain curve of native dragline silk. Fibers display an initial elastic modulus (the slope of the curve until the yielding point, arrow), after which plastic deformation occurs until breaking point (ultimate tensile strength, arrow). The area under the curve (shaded in grey) represents the toughness. Modified from Plaza *et al.* (2012).

The toughness differs between silk types and spider species, and also depends on environmental factors such as temperature, humidity, and spinning speed (Madsen *et al.*, 1999; Plaza *et al.*, 2006). The environmental factors cause high variability in tensile measurements, thereby making it difficult to say that one specific spider silk type is the toughest. Tensile properties obtained from only one spider species obtained under the same settings are displayed in Figure 8, to enable comparative analysis of tensile properties (Blackledge & Hayashi, 2006). These values are not to be seen as representative values of toughness for each spider silk type, but merely serve as a comparison of the different silk types within one species. In the study by Blackledge & Hayashi (2006), aciniform silk was determined the toughest silk type, due to a combination of high ultimate tensile strength and high extensibility.

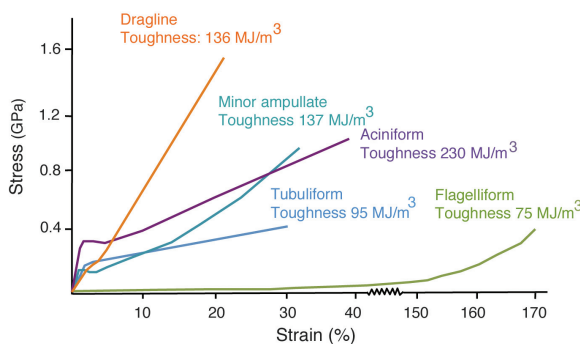


Figure 8. Representative stress/strain curves of the spider silk types discussed herein, and their respective toughness. Modified from Blackledge & Hayashi (2006).

Mechanical properties of spider silks are likely conferred by the secondary structures formed by the repetitive region. In dragline silk, poly-alanine blocks confer strength by forming strong  $\beta$ -sheets, and the glycine-rich repeats confer extensibility by forming  $3_1$ -helices (MaSp1) or  $\beta$ -turns (MaSp2) (Table 1) (Hayashi *et al.*, 1999). The variability in length and properties of the repetitive regions in different spider silk types and spider species is likely to explain some of the differences seen in mechanical properties (Gosline *et al.*, 1999). Aciniform silk is tougher than both dragline and minor ampullate silk, likely because it has a relatively high  $\beta$ -sheet content (giving high ultimate tensile strength) in combination with the presence of  $\beta$ -turns in the amorphous region (giving high extensibility) (Hayashi *et al.*, 2004; Blackledge & Hayashi, 2006). The outstanding extensibility of flagelliform silk is attributed to the abundance of proline-containing glycine-rich repeats in flagelliform spidroins that form  $\beta$ -turns and  $\beta$ -spirals (Table 1) (Blackledge & Hayashi, 2006).

## 1.2 Silkworm silk

Silkworms produce large amounts of silk for cocoons used during their metamorphosis from larvae to moths. Silkworm silk is studied for biotechnological and biomedical applications as reviewed by Omenetto and Kaplan (2010), and Altman *et al.*, (2003). When silkworm silk is to be used as a biomaterial, the silk is commonly regenerated from cocoons by processes involving boiling cocoons in water and dissolving the fibers in lithium bromide. Regeneration enables formulation of other formats for biomedical applications, such as films, foams, microcapsules, and hydrogels (Rockwood *et al.*, 2011). However, the regeneration process renders materials that are not similar to native silk in mechanical properties or structure (Hossain *et al.*, 2003; Plaza *et al.*, 2008; Koebley *et al.*, 2015). Further studies on the native silk formation process are therefore needed in order to realize more biomimetic spinning of silkworm silk fibers. The silkworm silk proteins (fibroins) and the spinning mechanisms in silkworms are introduced in the following paragraphs with main focus on the domesticated silkworm, *Bombyx mori*, as this is the most studied species and is also the species studied in Paper III.

### 1.2.1 Silkworm silk glands

Fibroins are produced and stored in silkworm silk glands that are believed to originate from salivary glands. The glands increase in size during five larval molts, reaching up to 15 cm in length in the fifth instar when the silk cocoons are spun (Perdrix-Gillot, 1979). The glands are paired, but their ducts fuse close to a pore on the lower lip, and one single fiber consisting of two fiber

filaments surrounded by a common outer sericin coat exits through the pore upon spinning (Magoshi *et al.*, 1993; Asakura *et al.*, 2007). The *B. mori* silk gland can be divided into three macroscopic parts: the posterior silk gland (PSG), the middle silk gland (MSG) and the anterior silk gland (ASG) (Figure 9) (Asakura *et al.*, 2007).

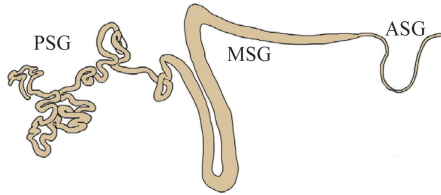


Figure 9. Schematic image of a *B. mori* silk gland, with posterior silk gland (PSG), middle silk gland (MSG), and anterior silk gland (ASG) denoted. Modified with permission from Paper III.

The cells in the PSG produce fibroins (Gamo *et al.*, 1977) that are stored in a soluble state at around 25% (w/v) in the MSG lumen (Laity *et al.*, 2015). The silk proteins are then transported through the ASG, and upon spinning, the fiber is pulled out by the motion of the silkworm's head (Vollrath & Knight, 2001).

The PSG and MSG of *B. mori* silk glands consist of a single columnar epithelial cell layer. Cells in the PSG and proximal part of the MSG are responsible for secreting fibroins (Magoshi *et al.*, 1993) while cells in the distal part of the MSG secrete different types of sericin. A cuticular intima, similar to the one described in major ampullate glands, lines the cuboidal epithelial cells in the ASG all the way to the lip pore (Asakura *et al.*, 2007). The diameter of the lumen in the ASG starts at around 400  $\mu\text{m}$ , and after a sudden drop to 100  $\mu\text{m}$  there is a slow decrease in diameter until it ends at around 50  $\mu\text{m}$  (Asakura *et al.*, 2007).

### 1.2.2 Silk formation in *Bombyx mori*

In analogy to spidroins, fibroins have been suggested to be stored as micelles (Jin & Kaplan, 2003; He *et al.*, 2012) or liquid crystals (Asakura *et al.*, 2007). A pH gradient along the gland is important for fiber formation, and has been proposed to go from 6.9 in the PSG, to around 5 in the MSG and down to 4.9 in the ASG. However, no details of the underlying experiments were described (Magoshi *et al.*, 1993). Another study showed that pH was 7-8 in the PSG and 5-6 in the MSG, while values of pH in the ASG were not determined (Miyake & Azuma, 2008). The pH gradient is dependent on ATPase-driven proton pumps in the silk gland epithelium (Azuma & Ohta, 1998).

Ion concentration gradients likely play a role in fiber formation in silkworms. Copper concentrations increase from the PSG to the ASG, and are significantly higher in the silk fiber compared to the end of the ASG (Zhou *et*

*al.*, 2003). Furthermore, levels of sodium, potassium, magnesium and zinc increase from PSG to ASG, while calcium levels decrease significantly (Zhou *et al.*, 2005). In analogy to spider silk glands, water reabsorption and shear forces in the ASG are important for the formation of a solid fiber and a stress-induced phase transition of the liquid spinning dope in the ASG leads to fiber formation (Asakura *et al.*, 2007).

### 1.2.3 Fibroins

Silkworm silk consists of several different proteins, the fibroin heavy (ca 350 kDa) and light chain (ca 25 kDa), and a polypeptide (P25) that associates to the heavy and light chain by hydrophobic interactions (Inoue *et al.*, 2000; Zhou *et al.*, 2000). The fibroin heavy chain is the main constituent of the silk, and consists of a hydrophilic N-terminal domain (FibNT) and a C-terminal segment (FibCT) flanking a repetitive region rich in glycine and alanine residues. The repetitive region contains twelve poly-glycine-alanine segments with short conserved linker sequences in between. The FibNT is 151 amino acid residues long (Zhou *et al.*, 2000) and adopts a random coil conformation at neutral pH, while a crystal structure solved at pH 4.7 reveals a dimer with anti-parallel  $\beta$ -sheets (He *et al.*, 2012). A cluster of acidic residues are probably protonated around pH 6, thereby inducing conformational changes in FibNT (He *et al.*, 2012). The FibCT is 58 residues long and links to the fibroin light chain via a disulfide bond. The secondary structure of FibCT has not been characterized but it has been suggested not to have a globular fold (Zhou *et al.*, 2001a). The fibroin light chain is non-repetitive and rich in arginine and lysine. Its function and importance has been debated but findings by Chen *et al.*, (2010) indicate that it plays an important role in lysine-mediated cross links in silk which might affect mechanical properties, while earlier studies have claimed that the fibroin light chain plays only a marginal role for the mechanical properties of the fiber (Zhou *et al.*, 2001a).

Soluble fibroins in the spinning dope contain repeated  $\beta$ -turns and random coils (Asakura *et al.*, 2001a; Asakura *et al.*, 2001b; Suzuki *et al.*, 2014). In the fiber state, the glycine-alanine-rich regions form  $\beta$ -sheets, while the linker regions form a more amorphous and flexible structure based on  $\beta$ -turns and random coils (Hayashi *et al.*, 1999; Asakura & Yao, 2002; Asakura *et al.*, 2002). The  $\beta$ -sheets in the silkworm silk fibers are mostly antiparallel (Zhou *et al.*, 2001a; Yao *et al.*, 2004), and the  $\beta$ -strands run parallel to the fiber axis (Zhou *et al.*, 2000).

#### 1.2.4 Mechanical properties of native silkworm silk

Forcibly reeled silk fibers from *B. mori* have an ultimate tensile strength of 0.6 GPa, a strain before breaking of 20%, and a toughness of around 70 MJ/m<sup>3</sup>. It is thus less tough than the spider silk types discussed herein (Figure 8) but is still tougher than Kevlar, and in the same range of toughness as Nylon (Gosline *et al.*, 1999). Shear forces are known to influence the structural transition from soluble proteins to solid fibers in both silkworms and spiders, but modelling suggests that the shear forces are much lower in the silkworm silk gland (Breslauer *et al.*, 2009), which might be one explanation to the inferior mechanical properties of silkworm silk compared to dragline silk. Another reason for why silkworm silk exhibits lower toughness levels than spider silk is that the primary structure of their repetitive regions is rather different (Xu & Lewis, 1990; Hinman & Lewis, 1992; Zhou *et al.*, 2001a). Silks with poly-glycine-alanine blocks are likely to have lower tensile strengths than those with poly-alanine blocks due to a difference in packing of the side chains in the  $\beta$ -sheet (Hayashi *et al.*, 1999).

### 1.3 Artificial spider silk

Since spiders cannot be used for large-scale production of spider silk, partial or full-length spidroins have to be expressed in heterologous hosts (Scheibel, 2004; Rising *et al.*, 2011; Chung *et al.*, 2012; Tokareva *et al.*, 2014). These recombinant proteins must then be purified, concentrated, and spun to obtain fibers. A highly concentrated spinning dope is needed to enable spinning of artificial spider silk, similar to the high spidroin concentration in the major ampullate gland (Hijirida *et al.*, 1996; Chen *et al.*, 2002). This means that the recombinant spidroin must not only have a high solubility, but there must also be substantial yields for the production to be economically feasible.

#### 1.3.1 Recombinant spidroins: purification and spinning

Recombinant spidroins can be produced in for example bacteria (Stark *et al.*, 2007; Teule *et al.*, 2009; Xia *et al.*, 2010; Albertson *et al.*, 2014; Heidebrecht *et al.*, 2015), yeast (Fahnestock *et al.*, 2000; Jansson, 2016), insect cells (Ittah *et al.*, 2006; Miao *et al.*, 2006), plants (Yang *et al.*, 2005; Peng *et al.*, 2016), or transgenic animals (Copeland *et al.*, 2015). The most widely used host is *Escherichia coli*, which is fairly easy to genetically modify, and represents a relatively cheap production system.

Many different recombinant spidroins have been expressed in *E. coli*, most of which have a marginal resemblance to their natural counterparts – lacking either one or both terminal domains and having a small repetitive region that

consists of iterated ensemble repeats (Table 2). Reasons for not expressing native-sized spidroins mostly lie in the fact that they are hard to produce in heterologous hosts because of their repetitive nature, size, and inherent propensity to assemble into fibers. Even when engineered smaller versions of recombinant miniature spider silk proteins (minispidroins) have been expressed, low yields (Stark *et al.*, 2007; Rammensee *et al.*, 2008; Gnesa *et al.*, 2012; Xu *et al.*, 2012) and low solubility (Bini *et al.*, 2006; Stark *et al.*, 2007; Rammensee *et al.*, 2008; Xu *et al.*, 2012; Zhang *et al.*, 2015) have been major obstacles.

Recombinant spidroins ranging from 24-285 kDa have been produced in *E. coli*, purified, and subsequently spun into fibers that have been characterized by tensile tests (Table 2). The highest specified yield from shake-flask cultures is 40 mg protein/L culture (Table 2) (Stark *et al.*, 2007; Lin *et al.*, 2013) while fermentor cultures have given up to 1500 mg protein/L culture (of a very small, 18 kDa protein) (Zhang *et al.*, 2015). One way to increase expression levels of spidroins in *E. coli* is to use bacterial strains that are modified to contain higher numbers of certain t-RNAs to account for the extreme abundance of some amino acid residues in the spidroin sequences. This enables improved expression of nearly native-sized recombinant spidroins (Xia *et al.*, 2010), but does not solve the problem with low solubility. To get soluble recombinant spidroins at a high concentration for spinning, recombinant spidroins are commonly dissolved in hexafluoroisopropanol (HFIP). However, even when dissolved in HFIP, spidroins display lower solubility levels than native spidroins, with concentrations of around 8-25% (Table 2) (Xia *et al.*, 2010; Lin *et al.*, 2013; Copeland *et al.*, 2015; Zhang *et al.*, 2015). Fusion to a non-spidroin solubility-enhancing partner is another way to increase solubility. Although it improves solubility of certain constructs (Stark *et al.*, 2007; Heidebrecht *et al.*, 2015), it has so far not been enough to reach the solubility of native spidroins. Moreover, the fusion partner often has to be removed, which may cause problems such as aggregation after cleaving off the fusion partner.

Currently, there are two main ways by which recombinant spidroins from *E. coli* are purified: (i) precipitation of *E. coli* proteins from a cell lysate using heat denaturation, followed by precipitation of the spidroins with ammonium sulfate. Next, precipitated spidroins are dissolved in guanidinium thiocyanate or guanidinium chloride, after which the sample is dialyzed, and the purified spidroin is freeze-dried (Fahnestock *et al.*, 2000; Huemmerich *et al.*, 2004), and (ii) centrifugation of the cell lysate followed by loading the supernatant containing the soluble recombinant spidroins (equipped with a polyhistidine tag) on an immobilized metal ion affinity chromatography (IMAC) column.

The histidine tag will bind to the matrix in the IMAC column, unwanted proteins are washed off, and the recombinant spideroin is eluted with an aqueous buffer (Stark *et al.*, 2007; Grip *et al.*, 2009; Heidebrecht *et al.*, 2015). The sample is dialyzed, possibly followed by freeze-drying (Teule *et al.*, 2009; Hsia *et al.*, 2012). To prepare concentrated spinning dopes, the freeze-dried spideroins from (i) or (ii) are commonly solubilized in for example HFIP (Teule *et al.*, 2009; Xia *et al.*, 2010; Hsia *et al.*, 2012; Adrianos *et al.*, 2013; Albertson *et al.*, 2014; Copeland *et al.*, 2015) or guanidinium-thiocyanate (Heidebrecht *et al.*, 2015). A few examples exist where aqueous buffers have been used for fiber formation, generally with very low protein concentration (Stark *et al.*, 2007; Xu *et al.*, 2012; Lin *et al.*, 2016).

Current methods to produce artificial fibers include electrospinning (Zhang *et al.*, 2015), hand-drawing (Teule *et al.*, 2007; Xu *et al.*, 2012; Lin *et al.*, 2016), wet spinning into coagulation baths (Xia *et al.*, 2010; Gnesa *et al.*, 2012; Hsia *et al.*, 2012; Adrianos *et al.*, 2013; Lin *et al.*, 2013; Albertson *et al.*, 2014; Copeland *et al.*, 2015; Heidebrecht *et al.*, 2015), gentle tilting in glass tubes (Stark *et al.*, 2007) or spinning through microfluidic devices (Rammensee *et al.*, 2008; Renberg *et al.*, 2014). As-spun fibers (fibers that have not been subjected to post-spinning manipulations) have normally been post-stretched to improve mechanical properties (Table 2). To post-stretch, as-spun fibers are cut into smaller pieces, after which they are stretched in different baths containing for example water and methanol (Xia *et al.*, 2010; Copeland *et al.*, 2015), isopropanol (Gnesa *et al.*, 2012; Albertson *et al.*, 2014; Copeland *et al.*, 2015; Heidebrecht *et al.*, 2015), or ethanol (Lin *et al.*, 2013).

**Table 2.** A comparison of native and recombinant spiderroins: expression, solubility, spinning method and mechanical properties. Published studies where recombinant spiderroins have been expressed and assembled in to fibers, which have been tested for mechanical properties are included. In publications where fibers made from several different recombinant spiderroins have been compared, the one with the highest toughness has been included in the table

NT	CT	Rep	Size (kDa)	Expression host	Expression yield	Solubility and solvent used	Fiber formation method and medium used	As-spun ultimate tensile strength (MPa)	As-spun strain (%)	As-spun Toughness (MJ/m <sup>2</sup> )	Post-stretching (X) and medium used	Post-stretched toughness (MJ/m <sup>2</sup> )
1	+	+	~300	n.a.	n.a.	30-50%, H <sub>2</sub> O	n.a.	1495 ± 65	20 ± 1	136 ± 7	n.a.	n.a.
2	-	+	64	<i>E. coli</i>	Shake flask 25 mg/L	n.s. K <sub>3</sub> PO <sub>4</sub>	Hand drawing Air	21 ± 1	28 ± 17	5 ± 3	n.s.	n.s.
3	+	+	76	<i>E. coli</i>	n.s.	n.s. Gdm-SCN	Wet spinning, 90% IPA	13 ± 2	6 ± 1	0.3 ± 0.1	6 75% IPA	189 ± 33 MJ/m <sup>3</sup>
4	-	-	95	<i>E. coli</i>	n.s.	n.s. Gdm-SCN	Wet spinning, 90% IPA	22 ± 4	22 ± 4	4 ± 1	675% IPA	110 ± 24 MJ/m <sup>3</sup>
5	-	+	65	Transgenic goats	n.s.	25% HFIP	Wet spinning, IPA	33 ± 7	1.1 ± 0.3	0.2 ± 0.1	1.5+1.5 80% IPA	123 ± 30 MJ/m <sup>3</sup>
6	-	-	80	<i>E. coli</i>	n.s.	48% HFIP	Wet spinning, IPA	14 ± 4	0.8 ± 0.3	0.06 ± 0.03	4 85% IPA	7 ± 9 MJ/m <sup>3</sup>
7	-	+	189	<i>E. coli</i>	Shake flask 40 mg/L	8-10% HFIP	Wet spinning, ZnCl <sub>2</sub> FeCl <sub>3</sub>	n.s.	n.s.	n.s.	5 Air + 50- 70% EtOH	310 MPa ~10% *

NT: N-terminal domain, CT: C-terminal domain, Rep: repetitive region, + indicates presence of domain, - indicates absence of domain, n.a.: not applicable, n.s.: not specified, HFIP: hexafluoroisopropanol, IPA: isopropylalcohol, Gdm-SCN: guanidinium-thiocyanate, EtOH: ethanol. X: the number of times the original length the fibers were post-stretched, \* toughness values have not been calculated. (1) Native dragline silk, *Argiope argentata* (Blackledge & Hayashi, 2006); (2) Aciniform and dragline silk *Argiope trifasciata*, FHF4 (Lin et al., 2016); (3) Dragline silk *Araneus diadematus*, N1L(AQ)<sub>12</sub>NR3. (Heidebrecht et al., 2015); (4) Dragline silk *A. diadematus*, (AQ)<sub>24</sub> (Heidebrecht et al., 2015); (5) Dragline silk, *Nephila clavipes* MaSp1/MaSp2 (Copeland et al., 2015); (6) Dragline silk, *Argiope aurantia* MaSp2, 1E (Albertson et al., 2014); (7) Tubuliform silk, *Nephila antipodiana*, 11RPC (Lin et al., 2013).

**Table 2 cont.** A comparison of native and recombinant spidroins: expression, solubility, spinning method and mechanical properties. Published studies where recombinant spidroins have been expressed and assembled in to fibers, which have been tested for mechanical properties are included. In publications where fibers made from several recombinant spidroins have been compared, the one with the highest toughness has been included in the table

NT	CT	Rep	Size (kDa)	Expression host	Expression yield	Solubility and solvent used	Fiber formation method and medium used	As-spun ultimate tensile strength (MPa)	As-spun strain (%)	As-spun toughness (MJ/m <sup>2</sup> )	Post-stretching (X) and medium used	Post-stretched toughness (MJ/m <sup>2</sup> )
8	-	-	66	<i>E. coli</i>	Shake flask 50 µg/L	15% HFIP	Wet spinning 100% IPA	0.7 ± 0.4	26 ± 18	0.06 ± 0.06	3 80% IPA	89 ± 24 MJ/m <sup>2</sup>
9	-	-	76	<i>E. coli</i>	Shake flask 22 mg/L	0.4% Tris-HCl	Hand drawing Air	115 ± 24	37 ± 11	34 ± 13	n.s.	n.s.
10	-	+	45	<i>E. coli</i>	Shake flask 7 mg/L	20% HFIP	Wet spinning 95% IPA	n.s.	n.s.	n.s.	3.5 75% IPA	21 ± 4 MJ/m <sup>2</sup>
11	-	-	285	<i>E. coli</i>	Fermentor 500 mg/L	20% HFIP	Wet spinning, MetOH	n.s.	n.s.	n.s.	5 90% MetOH	510 MPa 15 % *
12	-	+	24	<i>E. coli</i>	Shake flask 40 mg/L	0.6-2% Tris-HCl	Gentle tilting in glass tubes	n.s.	n.s.	n.s.	Two stretch- relax cycles Air	200 MPa 0.6-1% *
13	-	-	58	<i>E. coli</i>	Shake flask 7-10 mg/L	25% HFIP	Hand drawing Air	29 ± 8	19 ± 13	3.4 ± 2.6	n.s.	n.s.

NT: N-terminal domain, CT: C-terminal domain, Rep: repetitive region, + indicates presence of domain, - indicates absence of domain, n.s.: not specified, HFIP: hexafluoroisopropanol, IPA: isopropylalcohol, Gdm-SCN: guanidinium-thiocyanate, MetOH: methanol, X: the number of times the original length the fibers were post-stretched, \* toughness values have not been calculated. (8) Tubuliform silk *N. clavipes* GFY (Adrianos *et al.*, 2013) (9) Aciniform silk *A. trifasciata*, W4 (Xu *et al.*, 2012); (10) Tubuliform silk *Latrodectus hesperus*, TuSp1 1xC (Gnesa *et al.*, 2012); (11) Dragline silk, MaSp *N. clavipes* (Xia *et al.*, 2010); (12) Dragline silk, *E. australis* MaSp 4repCT (Stark *et al.*, 2007); (13) Flagelliform and dragline silk *N. clavipes*, Flag/MaSp2 A1S8<sub>20</sub> (Teule *et al.*, 2007).

### 1.3.2 Mechanical properties of artificial fibers

Most methods to produce artificial fibers have not yet produced fibers with mechanical properties equal to those of native spider silk. In fact, as-spun fibers commonly have toughness levels of only  $5 \text{ MJ/m}^3$  or less, which can be compared to levels of  $>100 \text{ MJ/m}^3$  for native dragline silk (Table 2, Figure 8) or  $>200 \text{ MJ/m}^3$  for aciniform silk (Figure 8). A hand-drawn fiber formed from recombinant aciniform spidroins reached an impressive toughness of  $34 \text{ MJ/m}^3$  (Table 2) without post-stretching. However, hand-drawing is not a suitable large-scale production method since only 10 cm long fibers could be produced (Xu *et al.*, 2012). In two studies where post-stretching of fibers in organic solvents was employed (Xia *et al.*, 2010; Heidebrecht *et al.*, 2015), fibers with toughness levels similar to native dragline silk were obtained. In Xia *et al.*, (2010) a native-sized recombinant MaSp (285 kDa) lacking terminal domains was expressed and purified under denaturing conditions, after which it was spun and post-stretched 500% in isopropanol. The stress/strain profile of the resulting fibers was very different from that of native spider silk (Xia *et al.*, 2010). In 2015, Heidebrecht and co-authors designed a 76 kDa recombinant spidroin (152 kDa dimer) containing both terminal domains and a short repetitive region from MaSp2. The spidroin was expressed in *E. coli*, purified under denaturing conditions, spun, and post-stretched 600% in isopropanol. Toughness levels were similar to native dragline silk, but the tensile behavior of the artificial fibers was quite different from native dragline silk with less strong and more extendible fibers (Heidebrecht *et al.*, 2015).

In all cases tested, post-stretching results in tougher fibers (Table 2) and smaller diameters of fibers, which may be associated with rearrangement of the molecules in the fiber (Copeland *et al.*, 2015; Heidebrecht *et al.*, 2015). This is presumed to be in analogy to native spidroins which are believed to change secondary structure not only due to the pH gradient, but also in response to shear forces that arise when the spinning dope flows through the duct upon pulling of the fiber (Knight *et al.*, 2000). However, it is unclear if the secondary structure of recombinant spidroins is altered upon post-stretching. In two recent studies, an increase in  $\beta$ -sheet content has been shown to occur after post-stretching (Copeland *et al.*, 2015; Heidebrecht *et al.*, 2015), while Albertson and coauthors (2014) did not see an increase in  $\beta$ -sheet content in their post-stretched fibers.

Considering the differences in mechanical properties of different native spider silks (Figure 8), it is likely that the use of ensemble repeats from different spidroin types in recombinant minispidroins will lead to differences in mechanical properties. However, from the studies outlined in Table 2, it is

difficult to conclude if this is true. Difficulties in drawing such conclusions mainly depend on large differences in purification and spinning strategies, and artificial fibers from different spiders or spider species have not been spun using the exact same setup (Table 2).

## 1.4 Carbonic anhydrase

Carbonic anhydrases (CA) constitute an enzyme family that is active in many physiological processes, such as acid-base balance, respiration, bone resorption and calcification, as reviewed by Chegwiddden & Carter (2000). The enzyme regulates intra- and extracellular concentrations of  $\text{CO}_2$ ,  $\text{HCO}_3^-$  and  $\text{H}^+$  by catalyzing the reversible reaction  $\text{CO}_2 + \text{H}_2\text{O} \leftrightarrow \text{HCO}_3^- + \text{H}^+$  and was first discovered by Stadie & O'Brien (1933) and Meldrum & Roughton (1933). In humans, CA-mediated movement of bicarbonate and bicarbonate-related species is important in for example regulation of blood pH and regulation of intracellular pH (Boron, 2010). Sixteen different CA isoforms have been described in humans, some of which are catalytically inactive (Frost & McKenna, 2014). The different isoforms have very low sequence similarity, but all catalytically active isoforms have an active site with a bound zinc ion. Carbonic anhydrases can also be grouped into different subtypes depending on the localization of the enzyme. The subtypes include cytosolic, mitochondrial, secreted, glycosyl-phosphatidylinositol-(GPI)-anchored, and transmembrane (Frost & McKenna, 2014).

Carbonic anhydrase is present extracellularly in the haemolymph of spiders (Stratakis & Linzen, 1984), but silk glands have never been analyzed for the presence of CA.

## 1.5 Amyloid

It has been suggested that the conversion from soluble spinning dope into a solid fiber in spiders and silkworms is similar to the formation of amyloid fibrils (Kenney *et al.*, 2002). Amyloids are fibrillar aggregates of proteins that form *in vivo* under physiological conditions (Sipe *et al.*, 2014). Amyloid formation is linked to more than 30 human diseases, such as Alzheimer's disease, Parkinson's disease, and type 2 diabetes, but there are also a growing number of examples of functional amyloid. Examples include antimicrobial human defensins that form amyloid-like fibril nano-nets at the gut mucosa, or bacteria being able to produce amyloid (curli) (Chapman *et al.*, 2002; Chu *et al.*, 2012; Bergman *et al.*, 2016).

Amyloid fibrils exhibit a characteristic cross- $\beta$  diffraction pattern, because the  $\beta$ -strands run perpendicular to the fiber axis (Nelson *et al.*, 2005; Sipe *et al.*, 2014; Landreh *et al.*, 2016). The definition of an amyloid fibril states that it is a rigid, non-branching fibril formed *in vivo*, which is around 10 nm in diameter, binds Congo red, and exhibits green, yellow or orange birefringence when viewed by polarization microscopy (Sipe *et al.*, 2014). Furthermore, amyloid fibrils bind Thioflavin T (ThT). The fluorescence of ThT changes upon binding to  $\beta$ -sheets, and a characteristic red-shift in wavelength of emission maximum can be detected, making it possible to follow the kinetics of amyloid fibril formation by ThT fluorescence spectroscopy (LeVine, 1993). Another hallmark of amyloid fibrils is that the addition of preformed fibrils (seeds) accelerates the kinetics of amyloid fibril formation which occurs through nucleation-dependent polymerization (Jucker & Walker, 2011). Fibrils that exhibit these properties but are formed *in vitro* are referred to as amyloid-like (Sipe *et al.*, 2014).

In analogy to amyloid formation, the secondary structure of spidroins and fibroins changes from  $\alpha$ -helical and random coil conformation to mainly  $\beta$ -sheet conformation under physiological conditions (Kenney *et al.*, 2002; Slotta *et al.*, 2007). Amyloid-like fibrils have been found in the lumen of the third limb of the s-shaped duct of the major ampullate gland, as visualized by TEM (Kenney *et al.*, 2002). Furthermore, *B. mori* silk acts as a seeding agent in the development of experimental amyloid protein A amyloidosis in mice (Lundmark *et al.*, 2005). There are no reports on the seeding capacity of native spider silk, but a minispidroin based on the repetitive region of the *A. diadematus* version of MaSp2 forms fibrils that are of similar size as amyloid fibrils, contains cross- $\beta$  structures (Slotta *et al.*, 2007), and is able to seed amyloid-like fibril assembly *in vitro* (Humenik *et al.*, 2015). Another minispidroin, based on the repetitive region and CT of *E. australis* MaSp1 was, however, not able to seed experimental amyloid protein A amyloidosis in mice (Tjernberg *et al.*, 2016). There are a few substantial differences between silk fibers and amyloid fibrils, including a difference in size (5-10 nm fibrils versus 1-6  $\mu\text{m}$  silk fibers) and the  $\beta$ -strands being parallel to the fiber axis in silk (van Beek *et al.*, 2002) while amyloids have a cross- $\beta$  structure (Nelson *et al.*, 2005).

## 2 Present investigation

### 2.1 Aims of this thesis

The overall aim of this thesis was to study the physiological conditions and molecular mechanisms that govern silk formation, to enable biomimetic spinning of artificial spider silk fibers. More specific aims were to:

- Study the cellular structures in major ampullate glands and localize NT in major ampullate glands and dragline silk (**Paper I**)
- Elucidate the mechanisms of native spider silk formation by determination of the pH and ion composition, as well as localization of CA activity, in major ampullate glands. Study the stability, fold, and interactions of the terminal domains of recombinant spidroins under the conditions found in the glands (**Paper II**)
- Study the cellular structures, determine the localization of CA activity and pH in *B. mori* silk glands (**Paper III**)
- Based on Papers I-III, design a miniature spidroin and a spinning device for biomimetic spinning of artificial spider silk fibers (**Paper IV**)

### 2.2 Materials and methods

Materials and methods used in this thesis that can benefit from clarification are described in more detail in this section. Detailed descriptions of all experimental procedures are presented in the respective papers.

### 2.2.1 Histochemical localization of carbonic anhydrase activity

Immunohistochemical studies of CA in spiders would be problematic because of the presence of many different CA isoforms, in combination with the fact that they have not been characterized in spiders. Ridderstrale has developed an elegant histochemical method that circumvents such problems, in that the activity of CA is detected irrespective of isoform (Ridderstrale, 1976; Ridderstrale, 1991).

Whole opisthosomas and isolated spider silk glands were embedded in Historesin, a water-soluble glycol methacrylate that allows for thinner sections than cryo- or paraffin-sections. For detection of CA activity, 2  $\mu\text{m}$  sections were incubated in a medium containing  $\text{NaHCO}_3$ ,  $\text{CoSO}_4$ ,  $\text{KH}_2\text{PO}_4/\text{Na}_2\text{HPO}_4$  and  $\text{H}_2\text{SO}_4$ . The  $\text{CO}_2$  produced due to the catalytic activity of CA (dehydration of  $\text{HCO}_3^-$ ) leaves the floating sections and thereby causes a local increase in pH at sites with CA activity, leading to formation of a cobalt-phosphate-carbonate complex. Next, sections were rinsed in phosphate buffer after which they were transferred to a blackening solution containing  $(\text{NH}_4)_2\text{S}$  which caused the cobalt-phosphate-carbonate complex to be converted into a black cobalt-sulfide precipitate (Ridderstrale, 1991). The sections were washed in distilled water and finally put on glass slides and counter-stained with Azure blue. For control of unspecific staining, some sections were incubated in the medium in presence of the CA inhibitor acetazolamide.

### 2.2.2 Determination of ion concentrations in silk glands

Concentric ion-selective microelectrodes (ISMs) were used to determine the concentrations of hydrogen, carbonate, sodium, potassium, and chloride ions in major ampullate glands (Paper II) and hydrogen ion concentration in silkworm silk glands (Paper III). For a detailed description of the construction of ISMs, see methods in Paper II. In short, the concentric microelectrodes consisted of two glass capillaries of different sizes, with the smaller capillary inserted into the larger capillary. The outer capillary had a tip diameter of 2-4  $\mu\text{m}$  and was filled with a 200  $\mu\text{m}$  column of liquid ion-selective cocktail. The inner capillary had a tip diameter of 1  $\mu\text{m}$ , was filled with KCl (3 M) and was inserted into the outer capillary with the tip positioned 4-6  $\mu\text{m}$  from the outer capillary tip (Figure 10). A silver wire coated with silver chloride was inserted in the inner capillary and connected to a voltage meter.

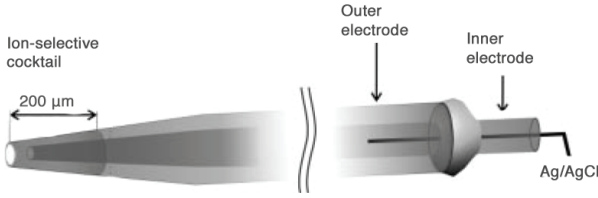


Figure 10. Schematic image of a concentric ion selective microelectrode. Modified from Fedirko *et al.*, (2006).

To illustrate how an electrode works, a hydrogen ion-selective microelectrode (*i.e.* a pH-electrode) is used as an example. When the electrode is submersed into a bath of known  $[H^+]$ , hydrogen ions will diffuse from the bath into the surface of the ion-selective cocktail. This will create a Nernst diffusion potential between the cocktail and the outside of the electrode, *i.e.* the bath, which can be recorded. Upon going from the bath to a solution of a different  $[H^+]$ , the diffusion potential will change ( $\Delta V$ ), according to the Nernst equation (Equation 1), and therefore the ( $\Delta V$ ) can be used to calculate the  $[H^+]$  of the unknown solution, knowing the pH of the bath and the slope response ( $m$ ) of the electrode. Subscripts 1 and 2 (in Equation 1) denote concentrations in starting and final solutions, respectively.

$$\Delta V = m \times \log \left( \frac{[\text{ion}]_2}{[\text{ion}]_1} \right) \quad (1)$$

In Paper II and III, silk glands were dissected in a modified Spider Ringer solution (Schartau & Leidescher, 1983) buffered with 26 mM  $HCO_3^-$  and 5%  $CO_2$ , after which the glands were mounted in a submersion-style chamber and superfused with modified Spider Ringer solution. A concentric ISM was lowered into the bath and a base line potential was recorded. Next, the ISM was inserted into the glandular lumen, and the potential was recorded. The shift in potential between the bath and glandular lumen was translated into change in ion concentration using the Nernst equation (Equation 1) (in the case of  $[H^+]$ ,  $[Na^+]$ ,  $[K^+]$ ,  $[Cl^-]$ ). To determine bicarbonate concentrations, a carbonate-selective ion cocktail was used. The reason for not using a bicarbonate-selective cocktail is that it in general has low selectivity for bicarbonate over carbonate. Instead, in combination with pH measurements, a carbonate-selective ion cocktail can be used, and the  $[CO_3^{2-}]$  can be calculated from the  $\Delta V$  between the bath and the lumen of the gland using a modified Nikolsky equation (Chesler *et al.*, 1994). The value of  $[HCO_3^-]$  in the gland lumen could then be calculated from the value of  $[CO_3^{2-}]$  and  $[H^+]$  using the equilibrium equation between carbonate and bicarbonate (Equation 2), where  $K_b$  is the bicarbonate dissociation constant.

$$[HCO_3^-] = \frac{[CO_3^{2-}][H^+]}{K_b} \quad (2)$$

Knowing the pH and  $[\text{HCO}_3^-]$ , the partial pressure of  $\text{CO}_2$  ( $\text{pCO}_2$ , in torr) in the tissue can be calculated using the Henderson-Hasselbalch equation (Equation 3), where  $K_c$  is a constant combining the apparent dissociation constant for carbonic acid and the solubility constant for  $\text{CO}_2$ , a value which was empirically determined in Chesler *et al.*, (1994) to 10.52 at 22°C.

$$(\text{pCO}_2) = [\text{HCO}_3^-] \times 10^{\text{p}K_c - \text{pH}} \quad (3)$$

Since the  $\text{pCO}_2$  in the lumen of the major ampullate gland was calculated to be very high, we questioned how such a high  $\text{pCO}_2$  could be maintained in the lumen, when carbon dioxide is generally considered able to diffuse freely across the cell membrane (Jacobs, 1920). To investigate this further, some glands were subjected to  $\text{CO}_2$  permeability studies. Glands were dissected, mounted, and superfused with Spider Ringer as described above. A pH electrode was inserted into the gland, after which the surrounding solution was exchanged to Spider Ringer buffered with 26 mM  $\text{HCO}_3^-$  and 100%  $\text{CO}_2$ . pH measurements within the lumen of the gland were continued up to one hour to see if intraluminal pH changed in response to the elevated  $\text{pCO}_2$  of the Ringer. To elucidate if it was the epithelium or the spinning dope that was impermeable to  $\text{CO}_2$ , two major ampullate glands were dissected as described previously, after which the epithelium was peeled off, leaving only the highly viscous spinning dope in the submersion-style chamber. A pH electrode was inserted into the dope, after which the dope was superfused with modified Spider Ringer (26 mM  $\text{HCO}_3^-$  and 100%  $\text{CO}_2$ ) and pH was monitored for 30 minutes, to see if the pH of the dope changed in response to the elevated  $\text{pCO}_2$ .

To study the influence of CA activity on the pH gradient, some glands were incubated in a membrane-permeable inhibitor of CA (methazolamide) for 30 minutes, after which the pH was measured. Next, the glands were incubated in Spider Ringer for 30 minutes to wash off the methazolamide, and pH measurements were repeated, to make sure that any change in pH upon treatment with methazolamide was not due to the cells dying, but only to the inhibition of CA.

### 2.2.3 Studies of recombinant NT and CT

In Paper II, a range of methods were used to study changes in stability and secondary structure of recombinant versions of *Araneus ventricosus* MiSp NT and *A. ventricosus* MiSp CT, some of which are outlined below.

### *Urea denaturation*

At a certain concentration, urea will unfold proteins to different extents depending on their stability. The higher the concentration of urea needed to denature a protein, the more stable the protein (Bennion & Daggett, 2003). In Paper II, urea denaturation was used as a tool to study the stability of recombinant NT and CT between pH 7.5 and 5.0. At each pH, urea denaturation curves were obtained by tryptophan fluorescence spectroscopy (for NT, which has one tryptophan residue, see further below) or CD spectroscopy (for CT).

### *Tryptophan fluorescence spectroscopy*

The amino acid residue tryptophan changes its fluorescence depending on its environment, as reviewed by Beechem & Brand (1985). Upon going from a hydrophobic to a more polar environment, there is a change in wavelength maximum seen as a red-shift in fluorescence. Tryptophan fluorescence spectroscopy can be used to study the dimerization of NT, since the tryptophan side chain goes from being buried in the monomer to being more solvent-exposed in the dimer. Since the environment of the tryptophan side-chain will change also upon denaturation of the protein, tryptophan fluorescence spectroscopy can also be used to study the stability of NT in presence of different concentrations of urea at different pHs. Data was analyzed by a two-state unfolding equation. For each measured pH, the transition point between the native and denatured state ([den]50%) was determined from plots of the tryptophan fluorescence ratio against the urea concentration. The transition points were then plotted as a function of pH.

### *Circular dichroism spectroscopy*

Circular dichroism spectroscopy can be used to study the secondary structure content of proteins. The technique is based on the difference in absorption of left- or right-handed circularly polarized light by chiral molecules such as proteins. The CD spectrum in the far-UV region (below 260 nm) is influenced by the conformation of the protein, and can be used to identify secondary structure contents. Using left- and right-handed circularly polarized light, a CD spectrometer measures the difference in absorption at the different wavelengths, from which the molar or mean residue ellipticity can be calculated. When the ellipticity is plotted against wavelengths ~190-260 nm, secondary structures such as  $\alpha$ -helices,  $\beta$ -sheets, and random coils will give rise to curves with characteristic minima and maxima (Greenfield & Fasman, 1969). Full CD spectra between 190 and 260 nm were recorded for NT and CT to study the shift in secondary structure upon lowering of pH. The residual

molar ellipticity was measured at 25, 45, 65, 85, and 95°C at pH 7.5, 6.5 or 5.5 respectively.

Circular dichroism spectroscopy can also be used to monitor the stability of a protein at different concentrations of urea, as well as to study thermal denaturation. In Paper II, CD spectroscopy was used to study urea denaturation of CT. At each pH, and different urea concentrations, the average ellipticity at 222 nm was obtained. The ellipticities at 222 nm for each pH was plotted against the urea concentration and fitted to a two-state unfolding model in order to determine the transition point between the native and denatured state ([den]50%) for each pH. The transition points were then plotted against pH. To study thermal denaturation, the temperature of the sample (recombinant NT or CT at pH 7.5, 6.5, or 5.5 respectively) was gradually increased and the signal at 222 nm was monitored, and later converted into mean residue ellipticity in  $\text{deg x cm}^2/\text{dmol}$  and plotted against temperature for each pH value tested.

#### *CO<sub>2</sub> analog interactions with the terminal domains*

In Paper II, the pCO<sub>2</sub> was calculated to be very high in the duct of major ampullate glands. The CT has previously been shown to undergo conformational changes in response to shear, resulting in increased exposure of non-polar surfaces (Hagn *et al.*, 2010). This, in combination with the fact that CO<sub>2</sub> interacts mainly with non-polar regions in proteins (van Lun, 2013), led us to study CO<sub>2</sub> interactions with NT and CT. A CO<sub>2</sub> analog (CS<sub>2</sub>) that is similar to CO<sub>2</sub> in size and shape (Wright *et al.*, 1992) was used to identify potential interaction sites in NT and CT. The rationale for using an analog was that CO<sub>2</sub> will affect the pH of the system, which is problematic since both the NT and CT used herein are pH-sensitive. The NT and CT were <sup>15</sup>N-labelled, and 2D <sup>15</sup>N-<sup>1</sup>H-HSQC spectra were recorded upon adding 0, 50, 100, and 200 mM CS<sub>2</sub> to the NMR sample, after which CS<sub>2</sub>-induced chemical shift perturbations were calculated.

#### *Mass spectrometry*

Mass spectrometry (MS) was used in Paper II and IV to study changes in the structure of recombinant NT and CT, and the minispidroin NT2RepCT, upon lowering the pH.

Hydrogen-deuterium exchange (HDX) MS can be used to study protein structural dynamics in solution by monitoring the exchange of backbone amide protons for deuterium from the solvent. The rate of exchange is dependent on solvent accessibility and local secondary structure, as reviewed by Englander (2006). In Paper II, we used HDX-MS to monitor the secondary structural changes of CT upon a lowering of pH. Time-dependent deuterium labelling of

CT was performed at pH 7.5, 6.5 or 5.5. Labelled protein was subsequently digested with pepsin and the resulting peptides were desalted and separated in a high-pressure liquid chromatography system and eluted directly into the mass spectrometer to quantify deuterium incorporation. Peptides were identified based on a map of undeuterated CT that had been acquired using liquid chromatography-tandem MS (LC-MS/MS).

Electrospray ionization (ESI) MS may be used to study intact protein molecules in the gas phase. In ESI-MS, drops of a protein solution are ionized and evaporated, leaving a charged species without solvent for intact mass analysis (Breuker & McLafferty, 2008). This approach, termed native MS, provides direct insights into the stoichiometries and dynamics of non-covalent protein complexes. In Paper IV we used ESI-MS to study the time-dependent assembly of recombinant NT, CT and NT2RepCT at pH 7.5 and 5.5. In addition, we used ESI-MS to study the stability of NT2RepCT fibrils in formic acid and acetonitrile to see if they behaved as amyloid-like fibrils, which are resistant to acetonitrile but readily dissociate in formic acid (Shen & Murphy, 1995).

#### 2.2.4 Tensile tests of artificial spider silk fibers

To perform tensile tests of artificial spider silk fibers, a fiber was mounted in a plastic frame with a gauge length of 20 mm. Accurate assessment of fiber diameter is very important, as this is used for calculation of stress (which is equal to force/surface area) (Hosford *et al.*, 2004). Traditionally, the diameter of spider silk fibers has been measured using scanning electron microscopy (Madsen *et al.*, 1999). In Paper IV, after being glued to the plastic frame, the diameter of individual fibers was measured in a light microscope, to avoid possible artefacts of the vacuum normally applied in scanning electron microscopy. The frames were mounted in a tensile tester, the sides of the plastic frame were cut and the stress and strain were measured. The stress/strain curves were used to calculate elastic modulus and toughness using the software Testwoks (MTS Systems Corporation Eden Prairie, USA).

## 2.3 Results

### 2.3.1 Paper I: Morphology and composition of the major ampullate gland and dragline silk

The tail and sac of the major ampullate gland were determined to consist of three different cell types, confined to three sharply demarcated zones, A-C (Figure 11). The cell types differed in epithelial cell height, position and shape of nuclei, as well as size, electron density, and affinity for haematoxylin-eosin and Azure blue of intracellular granules.

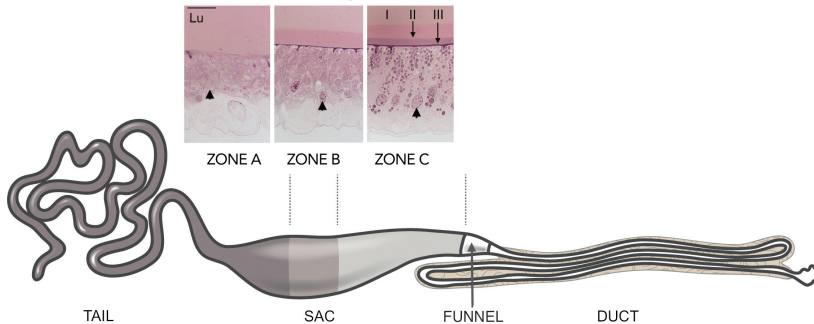


Figure 11. Schematic image of major ampullate gland, showing, from left to right, the tail, sac, funnel, and s-shaped duct. The three different zones (A–C) are indicated, and haematoxylin-eosin stained longitudinal sections of each zone are shown above the schematic image. Lu: lumen. I, II, and III represents three different layers added by the three different cell types. Arrow heads points to nuclei. Scale bar: 20  $\mu\text{m}$ . Modified with permission from Paper I.

The location of NT in *E. australis* major ampullate glands and dragline silk was analyzed by immuno-TEM using antibodies directed against recombinant *E. australis* MaSp1 NT. Immuno-staining of NT was found in the granules of the A and B zones, while the C zone granules did not stain for NT. This likely means that the A and B zone produce spidroins, while the C zone does not (at least not classical spidroins that include an NT). Two different layers were found in *E. australis* dragline silk, both likely containing spidroins, as indicated by the presence of NT in both layers.

### 2.3.2 Paper II: Carbonic anhydrase generates $\text{CO}_2$ and $\text{H}^+$ that drive spider silk formation via opposite effects on the terminal domains

By using a histochemical method, we showed that granules and the apical cell membrane of cells in the C zone of major ampullate glands contained active CA (Figure 12). Furthermore, the epithelial cells of all three limbs of the duct as well as the apical cell membrane and granules of epithelial cells in minor ampullate, aggregate and tubuliform glands, showed intense staining for CA activity.

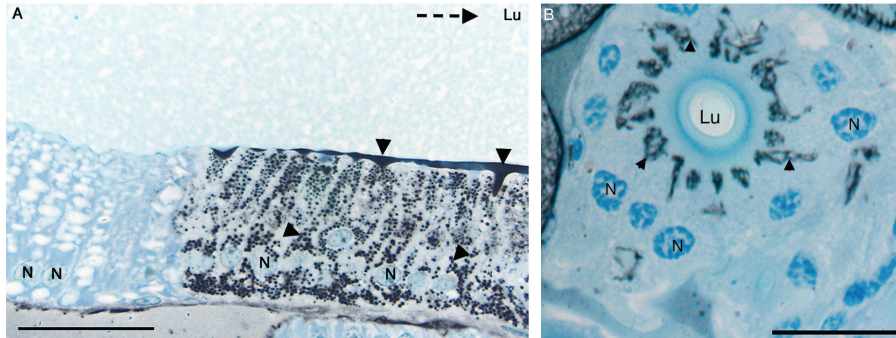


Figure 12. Carbonic anhydrase-activity (black precipitates, arrow heads) and Azure blue staining of major ampullate glands. (A) Longitudinal section of the sac, showing a sharp border between the B and C zone. The dotted arrow points towards the duct. (B) Cross-section of the third limb of the s-shaped duct. Lu: glandular lumen. N: nuclei. Scale bar (A) 50  $\mu\text{m}$ , (B) 20  $\mu\text{m}$ . Modified with permission from Paper II.

Next, the pH of major ampullate glands was measured using ion-selective microelectrodes. pH was determined to be 7.6 in the tail, 7.0 in the sac, and gradually lowered to 5.7 in the second limb of the major ampullate gland duct (Figure 13). The pH gradient reversibly collapsed upon treatment with the CA inhibitor methazolamide. A bicarbonate concentration gradient was also found along the tail and sac, going from 5 mM proximally to 21 mM distally (Figure 13). Assuming equilibrium conditions, an increasing bicarbonate level in combination with a decreasing pH imply an increasing  $\text{pCO}_2$  from the tail to the sac. Furthermore, the epithelium was determined to be impermeable for  $\text{CO}_2$ . At location 6 in Figure 13, ion concentrations of sodium, potassium and chloride were determined to be 192 mM, 6 mM and 164 mM respectively.

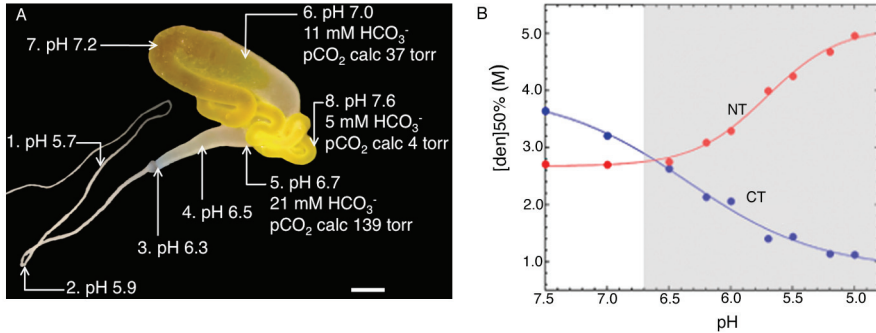


Figure 13. (A) Photograph of a major ampullate gland in which measured pH and  $[\text{HCO}_3^-]$  values and calculated  $\text{pCO}_2$  values at different locations are indicated. Scale bar: 1 mm. (B) Stability of N-terminal domain (NT) and C-terminal domain (CT) in 20 mM HEPES/MES buffer in the presence of 154 mM NaCl, measured with tryptophan fluorescence spectroscopy (NT) and CD spectroscopy (CT), presented as the molar urea concentration for apparent half-denaturation ( $[\text{den}]^{50\%}$ ) as a function of pH. The pH region in which CA activity is found in the gland is indicated by the shaded area. Modified with permission from Paper II.

Studies of NT and CT in isolation showed that the stability of NT was significantly increased while CT was destabilized when pH was changed from 7.5 to 5 (Figure 13). Thermal denaturation further showed that NT underwent a reversible transition from  $\alpha$ -helical conformation to being mainly unordered at all pH values studied, while CT irreversibly went from  $\alpha$ -helical to  $\beta$ -sheet conformation at pH 5.5, but not at pH 6.5 or 7.5. The HDX-MS analysis of CT showed increased HDX of helices 2, 3 and 5 at pH 5.5 compared to at pH 6.5 and pH 7.5, indicating an increased structural flexibility at lower pH.

A solution state NMR structure of *A. ventricosus* MiSp CT was determined and showed that CT folds into a five helix bundle and forms a constitutive parallel dimer at neutral pH. The fold is very similar to previously determined structures of *A. diadematus* MaSp CT (Hagn *et al.*, 2010) and *N. antipodiana* MiSp CT (Gao *et al.*, 2013) (Figure 14). When the pH is lowered, CT is gradually unfolded. The  $\text{CO}_2$  analog  $\text{CS}_2$  was found to interact specifically with a few, mainly hydrophobic CT residues distributed in helices 2-4, of which many are partially buried (Figure 14), which might promote unfolding of CT. No specific interactions between NT and  $\text{CS}_2$  were observed at low pH.

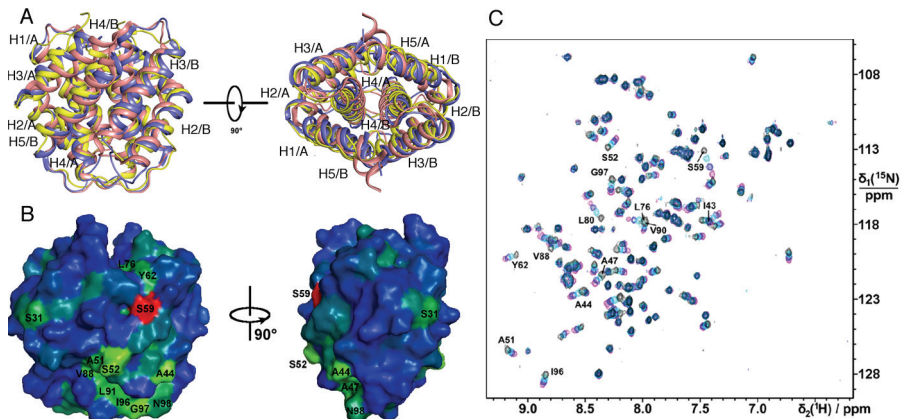


Figure 14. (A) Superposition of MiSp C-terminal domain (CT) structures from *A. ventricosus* (yellow), *N. antipodiana* (blue) and MaSp CT from *A. diadematus* (pink). Helices are shown as ribbons and labelled H1-H5. The letter A/B indicates the subunit. (B) Surface view of *A. ventricosus* MiSp CT, color-coded to reflect the backbone amide chemical shift perturbations upon addition of CS<sub>2</sub>, (red and green color corresponds to the most perturbed residues). (C) Overlay of 2D <sup>15</sup>N-<sup>1</sup>H-HSQC NMR spectra of MiSp CT with CS<sub>2</sub> added to concentrations of 0 mM (magenta), 50 mM (blue), 100 mM (cyan) and 200 mM (black). Reproduced with permission from Paper II.

Since CT converted to  $\beta$ -sheet structure at low pH, we further studied if CT formed amyloid-like fibrils at low pH. The CT converted to a ThT-positive state at pH 5.5 and below, which was not observed at a higher pH or for NT at any pH tested. Amyloid fibrils (5-10 nm in diameter) of CT were also observed by TEM, and they stained with Congo red and showed green birefringence under polarized light. From these studies it was proposed that NT dimerizes and gets more stable as pH is lowered, thereby interconnecting the spidroins (lock), while CT gets less stable and unfolds in response to low pH and high pCO<sub>2</sub> and turns into amyloid-like  $\beta$ -sheet nuclei from which further  $\beta$ -sheet formation of the spidroin repetitive region can take off (trigger). These features likely ensure that spidroins go from being soluble to forming insoluble fibers at the exact right time and place, thereby allowing rapid silk formation and avoiding precocious fiber assembly.

### 2.3.3 Paper III: Carbonic anhydrase generates a pH gradient in *Bombyx mori* silk glands

Four different epithelial cell types (I-IV) were found in *B. mori* silk glands, differing by the width and height of the columnar epithelial cells, as well as by their affinity for Azure blue and haematoxylin-eosin. Carbonic anhydrase activity was found in cell type IV which is present all along the ASG, and a pH gradient from 8.2 in the PSG to 6.2 in the beginning of the ASG was found (Figure 15). The pH gradient was dependent on the activity of CA, as indicated by the collapse of the pH gradient upon treatment with a CA inhibitor.

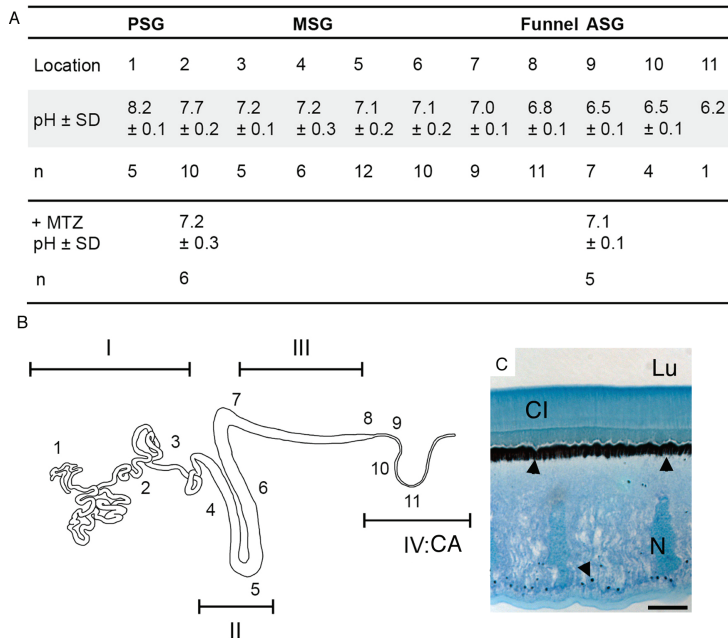


Figure 15. (A) Intraluminal pH of the silk gland was recorded at eleven locations (see schematic below Table) (B) Schematic image of a silk gland with locations for pH measurements and the different cell types I-IV indicated. Carbonic anhydrase (CA) activity was found in cell type IV. (C) In a longitudinal section of the ASG stained with Azure blue and stained for CA activity, black precipitates representing CA activity can be seen in intracellular granules and in microvilli at the apical cell membrane (arrow heads). PSG: posterior silk gland, MSG: middle silk gland, ASG: anterior silk gland, SD: standard deviation, n: number of glands measured, MTZ: methazolamide, CI: cuticular intima, Lu: lumen, N: nucleus. Modified with permission from Paper III.!!

### 2.3.4 Paper IV: Biomimetic spinning of artificial spider silk from an extremely concentrated chimeric minispidroin

The design of a chimeric recombinant minispidroin consisting of an NT and two ensemble repeats from *E. australis* MaSp1 and a CT derived from *A. ventricosus* MiSp (NT2RepCT) resulted in high expression in *E. coli*. Yields from shake flask cultures were 125 mg purified protein/L culture. Furthermore, NT2RepCT could be concentrated to >500 mg/ml in aqueous buffer (> 50%) which equals or even exceeds the protein concentration in the major ampullate gland. The high solubility was likely due to the presence of natively folded terminal domains, and the formation of micelles, as seen by cryo-EM and TEM. Upon a slight lowering of pH and induction of shear forces, NT2RepCT micelles fused and elongated.

Time-dependent assembly of NT, CT and NT2RepCT was studied with nESI-MS at pH 7.5 and pH 5.5. When pH was lowered to approximately 5.5, NT in isolation underwent rapid dimerization, while CT in isolation was gradually unfolded and dissociated into monomers. The NT2RepCT minispidroin was a dimer at neutral pH (as expected due to the constitutive dimeric nature of CT). Upon lowering of pH, oligomers of NT2RepCT could be seen for up to one minute, followed by the loss of signal indicating a pH-dependent multimerization of the minispidroin (Figure 16). The higher-order oligomers of NT2RepCT were amyloid-like, in the sense that they were not dissolved in acetonitrile, but required formic acid to dissociate into monomers (Figure 16) (Shen & Murphy, 1995).

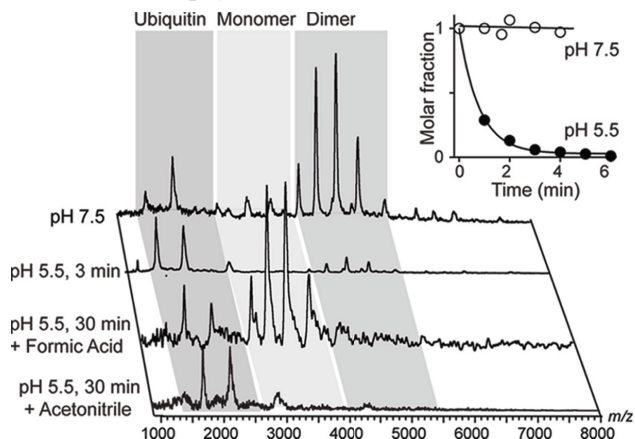


Figure 16. nESI-MS of, from top to bottom, NT2RepCT at pH 7.5, incubated at pH 5.5 for 3 min, incubated at pH 5.5 for 30 min and then dissolved in formic acid, and incubated at pH 5.5 for 30 min and then dissolved in acetonitrile. Ubiquitin was used as internal standard. Inset, fraction of NT2RepCT dimer over time at pH 7.5 (open symbols) and pH 5.5 (filled symbols).

When pumped through a pulled glass capillary into a low pH bath (between pH 3 and 5.5), the highly concentrated minispidroin formed a continuous fiber. Fibers could be collected in fiber nests in aqueous buffer or reeled up onto frames (Figure 17). A kilometer-long fiber could be spun from protein purified from one liter of shake flask bacterial culture. We further showed that commonly used methods to spin recombinant spidroins (spinning into coagulation baths with organic solvents) can generate fibers from proteins completely different from spidroins, such as bovine serum albumin. These fibers are not to be mistaken for being silk-like.

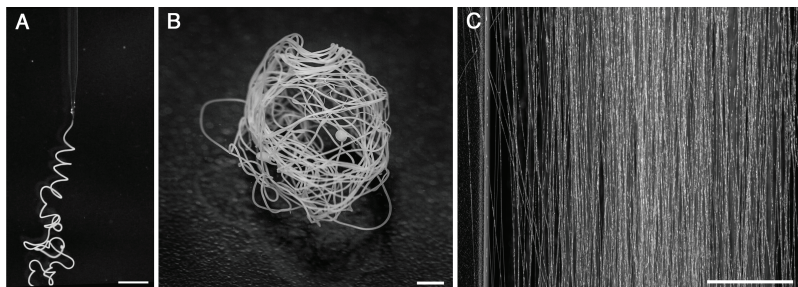


Figure 17. (A) Photo of a fiber as it is spun in a low pH aqueous collection bath. (B) Wet fiber nest in low pH buffer. (C) Fibers rolled up onto a frame. Fiber diameter in (A-B, wet) approximately 40  $\mu\text{m}$ . Fiber diameter in (C, dry) 15  $\mu\text{m}$ . Scale bar in (A) 3 mm (B-C) 5 mm.

The secondary structure of NT2RepCT changed upon spinning, going from mainly  $\alpha$ -helical and random coil to containing more  $\beta$ -sheet structures as determined by FTIR spectroscopy (Figure 18). As-spun NT2RepCT fibers exhibited qualitatively the same tensile behavior as native dragline silk, and they were highly reproducible (Figure 18). Fibers had an average ultimate tensile strength of 162 MPa, extensibility of 37 %, and toughness of 45 MJ/m<sup>3</sup>.

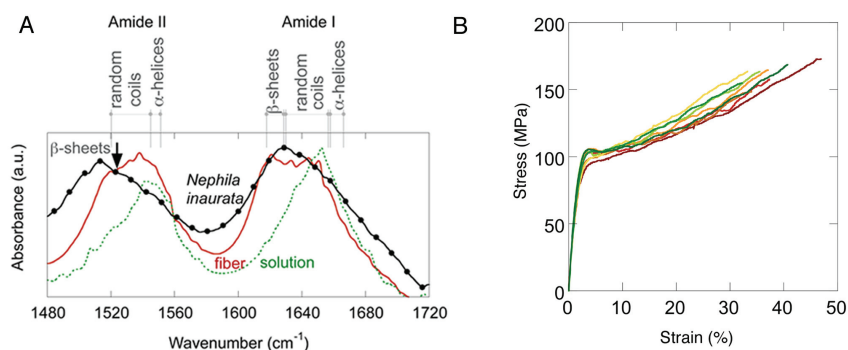


Figure 18. (A) Fourier transform infrared spectra of NT2RepCT in solution (dashed green) NT2RepCT fibers (red), and native dragline silk from *Nephila inaurata* (black) (B) Stress/strain curves of eight separate NT2RepCT fibers.

## 2.4 Discussion

### *Different cell types in silk glands*

Despite that the last common ancestor of spiders and silkworms existed more than 500 million years ago (Sanggaard *et al.*, 2014) there are remarkable similarities between the two with regards to the structural and functional properties of different parts of their glands. Both silkworm and spider silk glands consist of a single epithelial cell layer with very sharp borders between the different cell types in the epithelium. Studying the major ampullate glands using both TEM and LM enabled high resolution and the possibility of staining with different stains, respectively. Furthermore, the use of glutaraldehyde fixation followed by plastic embedding for LM for both types of glands resulted in improved preservation of the tissue and gave the possibility of obtaining thinner sections for LM, compared to for example LM, compared to for example paraformaldehyde-fixated and paraffin embedded tissue (Kovoor, 1987). These factors may explain why it was possible to discriminate three cell types in major ampullate glands (Paper I), as opposed to the previously seen two (Sponner *et al.*, 2007). In addition, NT was for the first time shown to be present in major ampullate glands and dragline silk, something that has been shown only for tubuliform spidroin NT previously (Hu *et al.*, 2006). The epithelium in both the major ampullate gland and the *B. mori* silk gland was shown to contain active CA, from the distal part of the sac/MSG and all along the duct/ASG (Paper II and Paper III).

### *pH and pCO<sub>2</sub> gradients in silk glands*

In Paper II we showed that CA supported a pH gradient along the major ampullate gland that was broader than previously determined. Previous studies have approximated pH, but measurements at precise locations have not been possible (Knight & Vollrath, 2001; Dicko *et al.*, 2004). Herein we used ion-selective microelectrodes with a tip size of only 2-4  $\mu\text{m}$ , which enabled reliable pH measurements at precise locations from the tail to half-way through the duct (Figure 19). The CA-supported pH gradient in silkworm silk glands was also different than previously determined, and the pH was higher at all locations measured than shown in a previous study (Magoshi *et al.*, 1993). It is difficult to speculate about the reasons for the discrepancy between our data and the data of Magoshi *et al.*, (1993) since the method to determine the pH gradient was not disclosed. The measured pH values in silk glands in Paper III did however correspond quite well to those approximated by phenol red injection into the haemocoel of silkworms (Miyake & Azuma, 2008). Proton pumps are vital for the generation of the pH gradient in both spiders and

silkworms (Vollrath *et al.*, 1998; Miyake & Azuma, 2008), and a combination of proton pumps and CA is probably needed to generate the low pH in the glands, since inhibition of proton pumps halts acidification, as does inhibition of CA. It was not possible to measure luminal pH all along the duct and ASG due to technical challenges, but pH is likely to drop further than determined herein since both CA activity and proton pumps were found all along the duct and ASG.

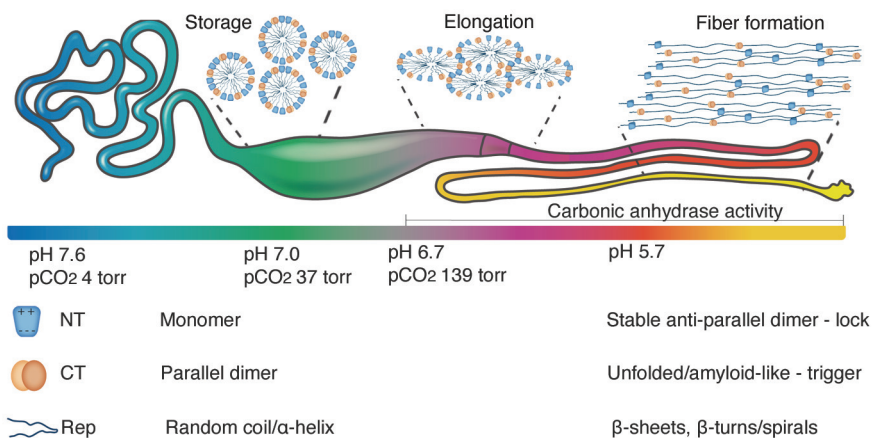


Figure 19. Schematic description of a major ampullate gland, and the different features involved in the transformation from soluble protein to a solid fiber. NT: N-terminal domain, CT: C-terminal domain, Rep: repetitive region, pCO<sub>2</sub>: calculated partial pressure of CO<sub>2</sub>. Data from Lefevre *et al.*, 2008; Askarieh *et al.*, 2010; Kronqvist *et al.*, 2014; Paper II; and Paper IV. Figure modified with permission from Macmillan Publishers Ltd: *Nature Chemical Biology* (Rising & Johansson, 2015) and (Kronqvist *et al.*, unpublished).

The concentration of carbonate ions at different sites in the lumen of major ampullate glands was also measured in Paper II. In combination with determined pH, these values were then used to calculate bicarbonate concentration and pCO<sub>2</sub>. Assuming equilibrium conditions within the lumen, the pCO<sub>2</sub> was very high in the distal part of the gland (Figure 19), and the epithelium was determined to be essentially impermeable to CO<sub>2</sub>. Carbon dioxide was early considered to diffuse freely across the cell membrane (Jacobs, 1920), but during the last decades, several studies have shown that this is not the case in all cells. For example, aquaporins have been suggested to act as CO<sub>2</sub> channels in the apical cell membrane of epithelial cells, as reviewed by Boron (2006) and Endeward *et al.*, (2014). A few documented examples of tissues with very low CO<sub>2</sub> permeability exist, such as gastric glands (Waisbren *et al.*, 1994), rat colonic crypts (Hasselblatt *et al.*, 2000) and guinea pig colon (Endeward & Gros, 2005). The mechanisms that mediate CO<sub>2</sub> impermeability

are not fully elucidated, but a high cholesterol content in the cell membrane can reduce CO<sub>2</sub> permeability (Itel *et al.*, 2012). How the epithelium of spider silk glands maintains a low CO<sub>2</sub> permeability remains to be determined, as does the putative existence of bicarbonate and pCO<sub>2</sub> gradients in silkworm silk glands.

#### *Lock and trigger model of spider silk formation*

We analyzed the stability and conformation of recombinant terminal domains upon lowering of pH from 7 to 5 and upon increasing the concentration of CS<sub>2</sub> (a CO<sub>2</sub> analog, Paper II). Upon lowering of pH, NT forms stable dimers, which interconnects the spidroins thereby allowing for the formation of large protein networks. We established that MiSp NT exhibits the same pH-dependent dimerization and stabilization (Paper II) as shown for MaSp NT (Kronqvist *et al.*, 2014), although it was later shown that the specific residues that are involved in the pH-sensitive relay differ. For example, a non-conserved glutamic acid residue (E73) is protonated instead of the conserved E84 in MaSp, and although no equivalent of the R60-D39 interaction pair in MaSp NT exists in MiSp NT there are three other inter-subunit charge interactions in that region (Otikovs *et al.*, 2015). The *N. clavipes* MaSp NT was recently determined to undergo pH-dependent dimerization in a similar manner as *E. australis* MaSp NT although the dimerization interface is somewhat different (Atkison *et al.*, 2016). Thus, the molecular mechanisms of NT seem to be conserved among different spider silk types and spider species (Kronqvist *et al.*, 2014; Otikovs *et al.*, 2015; Atkison *et al.*, 2016).

Due to the documented pH-insensitivity of recombinant MaSp CT (Askarieh *et al.*, 2010; Hagn *et al.*, 2010), we worked with MiSp CT for the studies in Paper II. Therein we showed, for the first time, that CT is pH-responsive under the conditions found in the gland, something which was confirmed also for *N. clavipes* MaSp CT shortly thereafter (Gauthier *et al.*, 2014). In response to low pH and high CS<sub>2</sub>, CT was destabilized, unfolded, and turned into  $\beta$ -sheet amyloid-like fibrils that possibly nucleate further  $\beta$ -sheet conversion of the repetitive region (Paper II). Structural rearrangement of CT has previously been determined to be accomplished by shear forces (Hagn *et al.*, 2010), and it is likely that a combination of shear forces and low pH will lead to unfolding of CT. The overall fold of MiSp CT determined by NMR was very similar to the fold of the MaSp CT studied by Hagn *et al.*, (2010), which is surprising considering the very different pH-dependency between the two. It is unclear if the insensitivity to pH observed for some CTs is due to a practical problem with heterologous production, or if CT has diverse functions in different silk types and spider species. It is still not fully elucidated which

amino acid residues in CT are protonated at low pH, but protonation of a glutamic acid in helix 4 (conserved among most MiSp CTs, Chen *et al.*, 2012) may be involved in pH-dependent unfolding of CT, by causing disruption of a salt bridge. Specific and partially buried residues in CT interacted with CS<sub>2</sub>, indicating that CO<sub>2</sub> might facilitate the unfolding of CT by interacting with mainly non-polar parts of CT. No specific interactions between NT and CS<sub>2</sub> were observed at low pH, suggesting that the formation of a stable NT dimer at low pH protects its hydrophobic residues from interacting with CO<sub>2</sub>.

Based on these results, we proposed a lock and trigger mechanism of spider silk formation in response to low pH and high pCO<sub>2</sub>, wherein NT dimerization leads to interlocking of spidroins into multimers (lock), while CT unfolds and turns into amyloid-like fibrils that can nucleate  $\beta$ -sheet formation of the repetitive region (trigger) (Figure 19). If so, this is to the best of our knowledge, the first example of where an increase in pCO<sub>2</sub> promotes unfolding of a protein. There are no known homologs to NT and CT, and the lock and trigger mechanism mediated by changes in pH and pCO<sub>2</sub> is therefore likely unique for spider silk formation. The presence of active CA not only in major ampullate glands but also in tubuliform and minor ampullate glands, in combination with NT and CT being highly conserved between different spidroins, indicate that the lock and trigger mechanism in response to a pH gradient could be universal for spinning of all spider silk types. The terminal domains of silkworm silk fibroins have not been studied as thoroughly as spidroins, and it is unclear if a similar lock and trigger mechanism governs silk formation also in silkworms.

### *Spinning of artificial fibers under denaturing conditions*

To date, many different partial or full-length spidroins have been expressed in a range of different hosts, and purified and spun into artificial fibers using different routes as outlined in Table 2. Most spidroins are expressed with very low yields, and none of the recombinant spidroins have fully replicated the solubility of native spidroins. Furthermore, the resulting fibers have not replicated the tensile behavior of native silk (Table 2). There are probably several explanations for this. Most published protocols entail freeze-drying of the recombinant spidroins, followed by solubilization in harsh solvents to generate artificial spinning dopes (Teule *et al.*, 2009; Xia *et al.*, 2010; Hsia *et al.*, 2012; Adrianos *et al.*, 2013; Lin *et al.*, 2013; Albertson *et al.*, 2014; Copeland *et al.*, 2015; Heidebrecht *et al.*, 2015; Zhang *et al.*, 2015). Next, fibers are wet-spun into a coagulation bath, possibly followed by post-stretching in an organic solvent. These processes denature the proteins, rendering them unable to assemble in a native-like manner. This is likely to

prevent spidroins from exhibiting a high solubility, folding into native structures, and forming tough fibers. Silk-like fibers are not likely to be formed under denaturing conditions, and in Paper IV we show that a protein completely unrelated to silk proteins forms continuous fibers when spun into a coagulation bath with organic solvents. Furthermore, most recombinant spidroins used today lack one or both terminal domains, which prohibits the possibility of native-like assembly into spidroin multimers. Considering the fine-tuned functions of NT and CT in increasing solubility at high pH, and in regulating fiber formation (as determined in Paper II), it is likely that silk-like fibers are impossible to spin from (i) constructs lacking NT and/or CT or (ii) denatured proteins.

#### *Biomimetic spinning of artificial spider silk*

Spider and silkworm silk have many excellent properties: they are tough, biodegradable, and relatively well-tolerated when implanted in living tissues (Vollrath *et al.*, 2002; Altman *et al.*, 2003; Allmeling *et al.*, 2008; Radtke *et al.*, 2011). For these reasons, silk has been claimed to be useful for many different industrial applications, but there is a need for large-scale production of biomimetic artificial silk fibers. It is apparent that spinning of native silks is a highly regulated and complicated matter that leads to specific refolding of the terminal domains and repetitive region. As a result, highly organized silk fibers with specific architectures are formed. An optimal biomimetic spinning approach is likely to depend on three main factors: (i) the design of a recombinant spidroin that includes both terminal domains and the repetitive region, exhibits high solubility, and is pH-sensitive; (ii) purification, storage and spinning processes that keep spidroins natively folded to allow for NT and CT to exert their functions in regulating fiber formation and (iii) the ability to mimic the spinning process, with *e.g.* lowered pH, ion exchange, dehydration, shearing and possibly a high pCO<sub>2</sub>.

#### *The design of a chimeric minispidroin that can form silk fibers in a biomimetic setup*

We noticed that not all recombinant versions of NT and CT exhibit high solubility and pH-sensitivity. For example, *E. australis* MaSp1 NT is highly soluble and pH-sensitive but *E. australis* MaSp1 CT is not very soluble and does not respond to pH (Askarieh *et al.*, 2010). The *A. ventricosus* MiSp CT on the other hand exhibits a very high solubility and is pH-sensitive (Paper II). Knowing that terminal domains from different species and spidroin types behave differently, we designed a chimeric minispidroin that included terminal domains that exhibit high solubility and pH sensitivity in isolation, as well as a

short repetitive region. The minispidroin in Paper IV multimerized upon lowering of pH, as demonstrated by nESI-MS, which detected oligomer formation during the first minute followed by the loss of signal (indicating higher order multimers). Thus, it is likely that the recombinant minispidroin in Paper IV is capable of native-like silk formation following the lock and trigger mechanism. The use of chimeric spidroins was discussed by Hinman *et al.*, (2000) and has been attempted a few times, but mainly to alter the mechanical properties of the artificial silk fibers by using ensemble repeats or separate motifs, from different spidroin types (Teule *et al.*, 2007; Teule *et al.*, 2012; Lin *et al.*, 2016). This is thus the first example of combining terminal domains from different spidroin types.

The chimeric minispidroin described in Paper IV exhibited equally high solubility as native spinning dopes, and could be spun into relatively tough fibers only by lowering pH. The unprecedented high solubility in aqueous buffer may be explained by the assembly of the minispidroin into micelles. The micelles fused and elongated upon a slight lowering of pH and induction of shear forces, similar to what has been shown for recombinant tubuliform spidroins (Lin *et al.*, 2009) and for fibroins in regenerated silkworm silk (Jin & Kaplan, 2003). Considering that NT dimerizes in an anti-parallel fashion, it is possible that NT subunits in different micelles pair up and dimerize upon lowering of pH, leading to interconnection of the micelles. Micelles are then likely to be elongated upon shearing (Paper II), ultimately leading to fiber formation (Figure 19).

To the best of our knowledge, the as-spun fibers in Paper IV are tougher than all other as-spun fibers, and are even tougher than some post-stretched fibers (Table 2). There are probably several explanations for this, including the high concentration of the spinning dope used, the biomimetic spinning as opposed to the use of denaturing conditions, and induction of shear forces along the spinning device. Most importantly, the inclusion of natively folded pH-responsive NT and CT likely means that silk formation is native-like where NT interconnects the spidroins and CT promotes re-folding of the repetitive region, which might result in improved tensile properties in contrast to recombinant spidroins that do not include the terminal domains.

### 3 Conclusions and outlook

- The single columnar epithelial cell layer in spider and silkworm silk glands can be divided into several sharply demarcated zones, each with a distinct epithelial cell type.
- Carbonic anhydrase upholds a broad pH gradient along spider and silkworm silk glands.
- Lowered pH and increased bicarbonate concentrations along the major ampullate gland, in combination with a CO<sub>2</sub> impermeable epithelium, imply that pCO<sub>2</sub> may reach high levels at the end of the duct.
- Spider silk formation is governed by a lock and trigger mechanism mediated by synchronous but opposite structural changes of NT and CT in response to lowering of pH.
- The design of a chimeric minispidroin with a short repetitive region and highly soluble and pH-responsive terminal domains from different spidroin types enables high expression levels and high protein solubility.
- The minispidroin assembles into fibers following the lock and trigger model when spun using a biomimetic spinning device that recapitulates the pH gradient and shear forces generated in spider silk glands.
- Protein purified from one liter shake flask bacterial culture is enough to spin a kilometer-long fiber that represents the hitherto toughest as-spun artificial spider silk fiber.

The spinning method and chimeric minispidroins described herein represent a breakthrough in the development of biomimetic spider silk fibers, and render well-defined fibers with reproducible mechanical properties. Considering how tough fibers we get herein with a very simple approach, it is highly likely that development of the process and the design of alternative chimeric minispidroins will enable us to spin even tougher fibers in the future. The existence of a vast amount of spidroin repetitive sequences that can be utilized

in chimeric minispidroins, means that opportunities to vary mechanical properties are many. The use of chimeric minispidroins and the biomimetic spinning process described herein offer a tool to: (i) spin fibers with tuneable mechanical properties by combining ensemble repeats from different spidroin types with highly soluble NT and CT, (ii) elucidate what mechanical properties specific motifs in the ensemble repeats of different native spidroins confer by including them in chimeric minispidroins and measuring tensile properties of the resulting fibers, and (iii) study the secondary and tertiary structures of the different motifs of the ensemble repeats in solution and in fiber state using solution and solid state NMR respectively.

Although we have come closer to understanding how spiders and silkworms spin their silk, there are still many unresolved questions. For example, how important is the presence of several different spidroins and other components in different types of spider silk, and is it a feature that is important to mimic in order to obtain artificial fibers that are true replicas of spider silk? It is well established that spidroins and fibroins are stored in secretory granula within epithelial cells after which they are secreted into the lumen of their respective gland. Silk proteins assemble in response to low pH, so how are they kept in solution in the presumably acidic secretory granula? What chaperone systems are involved in the secretory pathway, and can we use these so that native-sized recombinant spidroins and fibroins can be more efficiently expressed and purified under native conditions? Further fundamental studies of both spider and silkworm silk glands, and their corresponding silk types, could radically bring the field of silk biomimicry forward.

## 4 Populärvetenskaplig sammanfattning

Spindeltråd och silkesmasksilke är några av naturens mest fascinerande material - starka, men samtidigt lätta och biologiskt nedbrytbara. Spindeltråd tolereras också väl av kroppens vävnader, och möjliga användningsområden för spindeltråd sträcker sig från sjukvård till byggnadsindustri. Eftersom spindlar producerar små mängder tråd så måste vi tillverka konstgjord spindeltråd om den ska kunna användas i stor skala. Man har kunnat tillverka konstgjorda versioner av spindeltråd i ungefär ett decennium, men ingen har lyckats efterlikna spindeltrådens otroliga egenskaper. Målet med den här avhandlingen var därför att studera hur spindlar och silkesmaskar spinner sin tråd, för att sedan härma detta och utveckla en metod för att spinna tråd som liknar riktig spindeltråd.

Både spindeltråd och silkesmasksilke är gjort av proteiner som produceras i körtlar. Till skillnad från silkesmaskar som bara kan spinna en typ av tråd så kan spindlar producera flera olika typer av spindeltråd, alla med unika mekaniska egenskaper. Proteinerna är väldigt stora, och består generellt av tre delar: de N- och C-terminala domänerna, och däremellan den repetitiva regionen som består av ett fåtal olika varianter av amino-syror som är upprepade väldigt många gånger. Proteinerna förvaras i sina respektive körtlar vid hög koncentration i flytande form och spinns sedan till en tråd som dras ut genom en spinnvårta i spindelns bakdel, eller en por i silkesmaskens mun. Det har länge spekulerats i hur proteinerna kan vara i flytande form i en del av körteln, medan de väldigt snabbt kan bilda en tråd i en annan del av körteln.

Vi fann att dessa körtlar producerar ett enzym som kan göra omgivningen surare genom att omvandla koldioxid och vatten till bikarbonat och protoner. Enzymet hjälper till att skapa en pH- och koldioxid-gradient längs med körtlarna; det blir surare och högre tryck ju längre ut mot spinn-vårtan man kommer. Vidare studerade vi i detalj hur det låga pH-värdet och höga koldioxidtrycket påverkar spindeltrådsproteiner och kom fram till en "lock and

trigger"-modell. Den N-terminala domänen knyter ihop flera proteiner med varandra och skapar därmed ett nätverk av spindeltrådsproteiner vid lågt pH (lock), medan den C-terminala domänen bildar en struktur som kallas beta-lakan. Denna strukturomvandling påverkar troligtvis den repetitiva regionen så att även den ändrar struktur och bildar starka beta-lakan (trigger), vilket bidrar till styrkan i spindeltråden. Den väl kontrollerade pH-gradienten och "lock and trigger"-funktionen ser till att tråden inte bildas inne i körteln, men ändå kan bildas väldigt snabbt när spindeln spinner sin tråd.

Nästa mål med avhandlingen var att härma spindeln och silkesmasken och utveckla en biomimetisk process för att spinna konstgjord spindeltråd. Man har kunnat tillverka konstgjorda spindeltrådsproteiner ganska länge, men i små mängder, och för att spinna dem till tråd har man använt sig av starka kemikalier. De konstgjorda trådar som har bildats liknar inte spindeltråd, varken i styrka eller utseende. Problemet har legat i produktionen av proteinerna och i en otillräcklig förståelse av den naturliga spinningprocessen. I och med användandet av starka kemikalier under rening och spinning så fungerar inte den naturliga "lock and trigger"-regleringen och proteinerna klumpar ihop sig snarare än fogas samman på det kontrollerade sätt som sker i spindeln. Vi visade till exempel att man kan spinna tråd från proteiner som är väldigt olika spindeltrådsproteiner genom att spinna ut dem i sådana starka kemikalier.

I artikel IV beskriver vi tillverkandet av ett spindeltrådsprotein som består av de N- och C-terminala domänerna och en liten del av den repetitiva regionen. Vi lärde oss av studierna i artikel II att terminala domäner från vissa spindeltrådstyper är mer lösliga och pH-känsliga än andra, och vi designade därför ett chimärt protein där vi kombinerade domäner från olika spindeltrådstyper. Detta protein kunde tillverkas i stora mängder, och var mycket lösligt, stabilt, och pH-känsligt. Genom att konstruera en biomimetisk spinninganordning, bestående av en avsmalnande glaskapillär som slutar i en sur vattenlösning, gick det att spinna kilometer-långa trådar av spindeltrådsprotein. Den konstgjorda spindeltråden liknade riktig spindeltråd, och bildades genom en pH-reglerad "lock and trigger"-funktion. Detta motsvarar den allra första biomimetiska spinninganordningen för att spinna starka trådar från konstgjorda spindeltrådsproteiner.

## References

- Adrianos, S.L., Teule, F., Hinman, M.B., Jones, J.A., Weber, W.S., Yarger, J.L. & Lewis, R.V. (2013). Nephila clavipes Flagelliform silk-like GGX motifs contribute to extensibility and spacer motifs contribute to strength in synthetic spider silk fibers. *Biomacromolecules*, 14(6), pp. 1751-60.
- Albertson, A.E., Teule, F., Weber, W., Yarger, J.L. & Lewis, R.V. (2014). Effects of different post-spin stretching conditions on the mechanical properties of synthetic spider silk fibers. *J Mech Behav Biomed Mater*, 29, pp. 225-34.
- Allmeling, C., Jokuszies, A., Reimers, K., Kall, S., Choi, C.Y., Brandes, G., Kasper, C., Scheper, T., Guggenheim, M. & Vogt, P.M. (2008). Spider silk fibres in artificial nerve constructs promote peripheral nerve regeneration. *Cell Prolif*, 41(3), pp. 408-20.
- Altman, G.H., Diaz, F., Jakuba, C., Calabro, T., Horan, R.L., Chen, J., Lu, H., Richmond, J. & Kaplan, D.L. (2003). Silk-based biomaterials. *Biomaterials*, 24(3), pp. 401-16.
- Asakura, T., Ashida, J., Yamane, T., Kameda, T., Nakazawa, Y., Ohgo, K. & Komatsu, K. (2001a). A repeated beta-turn structure in poly(Ala-Gly) as a model for silk I of Bombyx mori silk fibroin studied with two-dimensional spin-diffusion NMR under off magic angle spinning and rotational echo double resonance. *J Mol Biol*, 306(2), pp. 291-305.
- Asakura, T., Umemura, K., Nakazawa, Y., Hirose, H., Higham, J. & Knight, D. (2007). Some observations on the structure and function of the spinning apparatus in the silkworm Bombyx mori. *Biomacromolecules*, 8(1), pp. 175-81.
- Asakura, T., Yamane, T., Nakazawa, Y., Kameda, T. & Ando, K. (2001b). Structure of Bombyx mori silk fibroin before spinning in solid state studied with wide angle x-ray scattering and <sup>13</sup>C cross-polarization/magic angle spinning NMR. *Biopolymers*, 58(5), pp. 521-5.
- Asakura, T. & Yao, J. (2002). <sup>13</sup>C CP/MAS NMR study on structural heterogeneity in Bombyx mori silk fiber and their generation by stretching. *Protein Sci*, 11(11), pp. 2706-13.
- Asakura, T., Yao, J., Yamane, T., Umemura, K. & Ulrich, A.S. (2002). Heterogeneous structure of silk fibers from Bombyx mori resolved by <sup>13</sup>C solid-state NMR spectroscopy. *J Am Chem Soc*, 124(30), pp. 8794-5.

- Askarieh, G., Hedhammar, M., Nordling, K., Saenz, A., Casals, C., Rising, A., Johansson, J. & Knight, S.D. (2010). Self-assembly of spider silk proteins is controlled by a pH-sensitive relay. *Nature*, 465(7295), pp. 236-8.
- Atkison, J.H., Parnham, S., Marcotte, W.R., Jr. & Olsen, S.K. (2016). Crystal Structure of the Nephila clavipes Major Ampullate Spidroin 1A N-terminal Domain Reveals Plasticity at the Dimer Interface. *J Biol Chem*, 291, pp. 19006-19017.
- Augsten, K., Muhlig, P. & Herrmann, C. (2000). Glycoproteins and skin-core structure in Nephila clavipes spider silk observed by light and electron microscopy. *Scanning*, 22(1), pp. 12-5.
- Ayoub, N.A., Garb, J.E., Tinghitella, R.M., Collin, M.A. & Hayashi, C.Y. (2007). Blueprint for a high-performance biomaterial: full-length spider dragline silk genes. *PLoS One*, 2(6), p. e514.
- Azuma, M. & Ohta, Y. (1998). Changes in H<sup>+</sup>-translocating vacuolar-type ATPase in the anterior silk gland cell of Bombyx mori during metamorphosis. *J Exp Biol*, 201(Pt 4), pp. 479-86.
- Beechem, J.M. & Brand, L. (1985). Time-resolved fluorescence of proteins. *Annu Rev Biochem*, 54, pp. 43-71.
- Bell, A.L. & Peakall, D.B. (1969). Changes in fine structure during silk protein production in the ampullate gland of the spider *Araneus sericatus*. *J Cell Biol*, 42, pp. 284-295.
- Bennion, B.J. & Daggett, V. (2003). The molecular basis for the chemical denaturation of proteins by urea. *Proc Natl Acad Sci U S A*, 100(9), pp. 5142-7.
- Bergman, P., Roan, N.R., Romling, U., Bevins, C.L. & Munch, J. (2016). Amyloid formation: functional friend or fearful foe? *J Intern Med*, 280(2), pp. 139-52.
- Bini, E., Foo, C.W., Huang, J., Karageorgiou, V., Kitchel, B. & Kaplan, D.L. (2006). RGD-functionalized bioengineered spider dragline silk biomaterial. *Biomacromolecules*, 7(11), pp. 3139-45.
- Blackledge, T.A. & Hayashi, C.Y. (2006). Silken toolkits: biomechanics of silk fibers spun by the orb web spider *Argiope argentata* (Fabricius 1775). *J Exp Biol*, 209(Pt 13), pp. 2452-61.
- Bon, M. (1710). A Discourse upon the Usefulness of the Silks of Spiders. By Monsieur Bon, President of the Court of Accounts, Aydes and Finances, and President of the Royal Society of Sciences at Montpellier. Communicated by the Author. *Philosophical Transactions*, 27, pp. 2-16.
- Boron, W.F. (2006). Acid-base transport by the renal proximal tubule. *J Am Soc Nephrol*, 17(9), pp. 2368-82.
- Boron, W.F. (2010). Evaluating the role of carbonic anhydrases in the transport of HCO<sub>3</sub><sup>-</sup>-related species. *Biochim Biophys Acta*, 1804(2), pp. 410-21.
- Breslauer, D.N., Lee, L.P. & Muller, S.J. (2009). Simulation of flow in the silk gland. *Biomacromolecules*, 10(1), pp. 49-57.
- Breuker, K. & McLafferty, F.W. (2008). Stepwise evolution of protein native structure with electrospray into the gas phase, 10(-12) to 10(2) s. *Proc Natl Acad Sci U S A*, 105(47), pp. 18145-52.
- Casem, M.L., Tran, L.P. & Moore, A.M. (2002). Ultrastructure of the major ampullate gland of the black widow spider, *Latrodectus hesperus*. *Tissue Cell*, 34(6), pp. 427-36.
- Chapman, M.R., Robinson, L.S., Pinkner, J.S., Roth, R., Heuser, J., Hammar, M., Normark, S. & Hultgren, S.J. (2002). Role of *Escherichia coli* curli operons in directing amyloid fiber formation. *Science*, 295(5556), pp. 851-5.

- Chegwidden, W.R. & Carter, N.D. (2000). Introduction to the carbonic anhydrases. *Exs*(90), pp. 14-28.
- Chen, G., Liu, X., Zhang, Y., Lin, S., Yang, Z., Johansson, J., Rising, A. & Meng, Q. (2012). Full-length minor ampullate spidroin gene sequence. *PLoS One*, 7(12), p. e52293.
- Chen, W.Q., Prievalder, H., John, J.P. & Lubec, G. (2010). Silk cocoon of *Bombyx mori*: proteins and posttranslational modifications--heavy phosphorylation and evidence for lysine-mediated cross links. *Proteomics*, 10(3), pp. 369-79.
- Chen, X., Knight, D.P. & Vollrath, F. (2002). Rheological characterization of nephila spidroin solution. *Biomacromolecules*, 3(4), pp. 644-8.
- Chesler, M., Chen, J.C. & Kraig, R.P. (1994). Determination of extracellular bicarbonate and carbon dioxide concentrations in brain slices using carbonate and pH-selective microelectrodes. *J Neurosci Methods*, 53(2), pp. 129-36.
- Chu, H., Pazgier, M., Jung, G., Nuccio, S.P., Castillo, P.A., de Jong, M.F., Winter, M.G., Winter, S.E., Wehkamp, J., Shen, B., Salzman, N.H., Underwood, M.A., Tsois, R.M., Young, G.M., Lu, W., Lehrer, R.I., Baumler, A.J. & Bevins, C.L. (2012). Human alpha-defensin 6 promotes mucosal innate immunity through self-assembled peptide nanonets. *Science*, 337(6093), pp. 477-81.
- Chung, H., Kim, T.Y. & Lee, S.Y. (2012). Recent advances in production of recombinant spider silk proteins. *Curr Opin Biotechnol*, 23(6), pp. 957-64.
- Copeland, C.G., Bell, B.E., Christensen, C.D. & Lewis, R.V. (2015). Development of a Process for the Spinning of Synthetic Spider Silk. *ACS Biomater Sci Eng*, 1(7), pp. 577-584.
- Davies, G.J., Knight, D.P. & Vollrath, F. (2013). Structure and function of the major ampullate spinning duct of the golden orb weaver, *Nephila edulis*. *Tissue Cell*, 45(5), pp. 306-11.
- Dicko, C., Vollrath, F. & Kenney, J.M. (2004). Spider silk protein refolding is controlled by changing pH. *Biomacromolecules*, 5(3), pp. 704-10.
- Eisoldt, L., Thamm, C. & Scheibel, T. (2011). Review the role of terminal domains during storage and assembly of spider silk proteins. *Biopolymers*, 97(6), pp. 355-61.
- Endeward, V., Al-Samir, S., Itel, F. & Gros, G. (2014). How does carbon dioxide permeate cell membranes? A discussion of concepts, results and methods. *Front Physiol*, 4, p. 382.
- Endeward, V. & Gros, G. (2005). Low carbon dioxide permeability of the apical epithelial membrane of guinea-pig colon. *J Physiol*, 567(Pt 1), pp. 253-65.
- Englander, S.W. (2006). Hydrogen exchange and mass spectrometry: A historical perspective. *J Am Soc Mass Spectrom*, 17(11), pp. 1481-9.
- Fahnestock, S.R., Yao, Z. & Bedzyk, L.A. (2000). Microbial production of spider silk proteins. *J Biotechnol*, 74(2), pp. 105-19.
- Fedirko, N., Svichar, N. & Chesler, M. (2006). Fabrication and use of high-speed, concentric h<sup>+</sup>- and Ca<sup>2+</sup>-selective microelectrodes suitable for in vitro extracellular recording. *J Neurophysiol*, 96(2), pp. 919-24.
- Frische, S., Maunsbach, A.B. & Vollrath, F. (1998). Elongate cavities and skin-core structure in *Nephila* spider silk observed by electron microscopy. *Journal of Microscopy*, 189(1), pp. 64-70.
- Frost, S.C. & McKenna, R. (eds) (2014). *Carbonic Anhydrase: Mechanism, Regulation, Links to Disease, and Industrial Applications*. (Subcellular Biochemistry, 75): Springer.

- Gaines, W.A., Sehorn, M.G. & Marcotte, W.R., Jr. (2010). Spidroin N-terminal domain promotes a pH-dependent association of silk proteins during self-assembly. *J Biol Chem*, 285(52), pp. 40745-53.
- Gamo, T., Inokuchi, T. & Laufer, H. (1977). Polypeptides of fibroin and sericin secreted from the different sections of the silk gland in *Bombyx mori*. *Insect Biochem*, 7(3), pp. 285-295.
- Gao, Z., Lin, Z., Huang, W., Lai, C.C., Fan, J.S. & Yang, D. (2013). Structural characterization of minor ampullate spidroin domains and their distinct roles in fibroin solubility and fiber formation. *PLoS One*, 8(2), p. e56142.
- Garb, J.E., Ayoub, N.A. & Hayashi, C.Y. (2010). Untangling spider silk evolution with spidroin terminal domains. *BMC Evol Biol*, 10, p. 243.
- Gauthier, M., Leclerc, J., Lefevre, T., Gagne, S.M. & Auger, M. (2014). Effect of pH on the structure of the recombinant C-terminal domain of *Nephila clavipes* dragline silk protein. *Biomacromolecules*, 15(12), pp. 4447-54.
- Giesa, T., Perry, C.C. & Buehler, M.J. (2016). Secondary Structure Transition and Critical Stress for a Model of Spider Silk Assembly. *Biomacromolecules*, 17(2), pp. 427-36.
- Gnesa, E., Hsia, Y., Yarger, J.L., Weber, W., Lin-Cereghino, J., Lin-Cereghino, G., Tang, S., Agari, K. & Vierra, C. (2012). Conserved C-terminal domain of spider tubuliform spidroin 1 contributes to extensibility in synthetic fibers. *Biomacromolecules*, 13(2), pp. 304-12.
- Gosline, J.M., Guerette, P.A., Ortlepp, C.S. & Savage, K.N. (1999). The mechanical design of spider silks: from fibroin sequence to mechanical function. *J Exp Biol*, 202, pp. 3295-3303.
- Gould, S.A., Tran, K.T., Spagna, J.C., Moore, A.M. & Shulman, J.B. (1999). Short and long range order of the morphology of silk from *Latrodectus hesperus* (Black Widow) as characterized by atomic force microscopy. *Int J Biol Macromol*, 24(2-3), pp. 151-7.
- Greenfield, N. & Fasman, G.D. (1969). Computed circular dichroism spectra for the evaluation of protein conformation. *Biochemistry*, 8(10), pp. 4108-16.
- Grip, S., Johansson, J. & Hedhammar, M. (2009). Engineered disulfides improve mechanical properties of recombinant spider silk. *Protein Sci*, 18(5), pp. 1012-22.
- Hagn, F., Eisoldt, L., Hardy, J.G., Vendrely, C., Coles, M., Scheibel, T. & Kessler, H. (2010). A conserved spider silk domain acts as a molecular switch that controls fibre assembly. *Nature*, 465(7295), pp. 239-42.
- Hagn, F., Thamm, C., Scheibel, T. & Kessler, H. (2011). pH-dependent dimerization and salt-dependent stabilization of the N-terminal domain of spider dragline silk--implications for fiber formation. *Angew Chem Int Ed Engl*, 50(1), pp. 310-3.
- Hasselblatt, P., Warth, R., Schulz-Baldes, A., Greger, R. & Bleich, M. (2000). pH regulation in isolated in vitro perfused rat colonic crypts. *Pflugers Arch*, 441(1), pp. 118-24.
- Hayashi, C.Y., Blackledge, T.A. & Lewis, R.V. (2004). Molecular and mechanical characterization of aciniform silk: uniformity of iterated sequence modules in a novel member of the spider silk fibroin gene family. *Mol Biol Evol*, 21(10), pp. 1950-9.
- Hayashi, C.Y. & Lewis, R.V. (1998). Evidence from flagelliform silk cDNA for the structural basis of elasticity and modular nature of spider silks. *J Mol Biol*, 275(5), pp. 773-84.
- Hayashi, C.Y., Shipley, N.H. & Lewis, R.V. (1999). Hypotheses that correlate the sequence, structure, and mechanical properties of spider silk proteins. *Int J Biol Macromol*, 24(2-3), pp. 271-5.

- He, Y.X., Zhang, N.N., Li, W.F., Jia, N., Chen, B.Y., Zhou, K., Zhang, J., Chen, Y. & Zhou, C.Z. (2012). N-Terminal domain of Bombyx mori fibroin mediates the assembly of silk in response to pH decrease. *J Mol Biol*, 418(3-4), pp. 197-207.
- Hedhammar, M., Rising, A., Grip, S., Martinez, A.S., Nordling, K., Casals, C., Stark, M. & Johansson, J. (2008). Structural properties of recombinant nonrepetitive and repetitive parts of major ampullate spidroin 1 from Euprostheno australis: implications for fiber formation. *Biochemistry*, 47(11), pp. 3407-17.
- Heidebrecht, A., Eisoldt, L., Diehl, J., Schmidt, A., Geffers, M., Lang, G. & Scheibel, T. (2015). Biomimetic fibers made of recombinant spidroins with the same toughness as natural spider silk. *Adv Mater*, 27(13), pp. 2189-94.
- Hijirida, D.H., Do, K.G., Michal, C., Wong, S., Zax, D. & Jelinski, L.W. (1996). <sup>13</sup>C NMR of Nephila clavipes major ampullate silk gland. *Biophys J*, 71(6), pp. 3442-7.
- Hinman, M., Dong, Z., Xu, M. & Lewis, R.V. (1992). Spider silk: a mystery starting to unravel. *Results Probl Cell Differ*, 19, pp. 227-54.
- Hinman, M.B., Jones, J.A. & Lewis, R.V. (2000). Synthetic spider silk: a modular fiber. *Trends Biotechnol*, 18(9), pp. 374-9.
- Hinman, M.B. & Lewis, R.V. (1992). Isolation of a clone encoding a second dragline silk fibroin. Nephila clavipes dragline silk is a two-protein fiber. *J Biol Chem*, 267(27), pp. 19320-4.
- Holland, G.P., Creager, M.S., Jenkins, J.E., Lewis, R.V. & Yarger, J.L. (2008). Determining secondary structure in spider dragline silk by carbon-carbon correlation solid-state NMR spectroscopy. *J Am Chem Soc*, 130(30), pp. 9871-7.
- Hosford, W.F., Mumford, P.M. & Gedney, R. (2004). Introduction to tensile testing. In: *Tensile Testing*. 2nd. ed. Ohio: American Technical Publishers Ltd.
- Hossain, K.S., Ochi, A., Ooyama, E., Magoshi, J. & Nemoto, N. (2003). Dynamic light scattering of native silk fibroin solution extracted from different parts of the middle division of the silk gland of the Bombyx mori silkworm. *Biomacromolecules*, 4(2), pp. 350-9.
- Hronska, M., van Beek, J.D., Williamson, P.T., Vollrath, F. & Meier, B.H. (2004). NMR characterization of native liquid spider dragline silk from Nephila edulis. *Biomacromolecules*, 5(3), pp. 834-9.
- Hsia, Y., Gnesa, E., Pacheco, R., Kohler, K., Jeffery, F. & Vierra, C. (2012). Synthetic spider silk production on a laboratory scale. *J Vis Exp*(65), p. e4191.
- Hu, X., Kohler, K., Falick, A.M., Moore, A.M., Jones, P.R. & Vierra, C. (2006). Spider egg case core fibers: trimeric complexes assembled from TuSp1, ECP-1, and ECP-2. *Biochemistry*, 45(11), pp. 3506-16.
- Huemmerich, D., Helsen, C.W., Quedzuweit, S., Oschmann, J., Rudolph, R. & Scheibel, T. (2004). Primary structure elements of spider dragline silks and their contribution to protein solubility. *Biochemistry*, 43(42), pp. 13604-12.
- Humenik, M., Smith, A.M., Arndt, S. & Scheibel, T. (2015). Ion and seed dependent fibril assembly of a spidroin core domain. *J Struct Biol*, 191(2), pp. 130-8.
- Inoue, S., Tanaka, K., Arisaka, F., Kimura, S., Ohtomo, K. & Mizuno, S. (2000). Silk fibroin of Bombyx mori is secreted, assembling a high molecular mass elementary unit consisting of H-chain, L-chain, and P25, with a 6:6:1 molar ratio. *J Biol Chem*, 275(51), pp. 40517-28.

- Itel, F., Al-Samir, S., Oberg, F., Chami, M., Kumar, M., Supuran, C.T., Deen, P.M., Meier, W., Hedfalk, K., Gros, G. & Endeward, V. (2012). CO<sub>2</sub> permeability of cell membranes is regulated by membrane cholesterol and protein gas channels. *FASEB J*, 26(12), pp. 5182-91.
- Ittah, S., Cohen, S., Garty, S., Cohn, D. & Gat, U. (2006). An essential role for the C-terminal domain of a dragline spider silk protein in directing fiber formation. *Biomacromolecules*, 7(6), pp. 1790-5.
- Jacobs, M.H. (1920). To what extent are the physiological effects of carbon dioxide due to hydrogen ions? *Am J Physiol*, 51, pp. 321-331.
- Jansson, J., Lau, C.H., Ishida, T., Ramström, M., Sandgren, M., Hedhammar, M. (2016). Functionalized silk assembled from a recombinant spider silk fusion protein (Z-4RePCT) produced in the methylotrophic yeast *Pichia pastoris*. *Biotechnol J*, 11(5), pp. 687-699.
- Jaudzems, K., Askarieh, G., Landreh, M., Nordling, K., Hedhammar, M., Jornvall, H., Rising, A., Knight, S.D. & Johansson, J. (2012). pH-dependent dimerization of spider silk N-terminal domain requires relocation of a wedged tryptophan side chain. *J Mol Biol*, 422(4), pp. 477-87.
- Jenkins, J.E., Creager, M.S., Butler, E.B., Lewis, R.V., Yarger, J.L. & Holland, G.P. (2010). Solid-state NMR evidence for elastin-like beta-turn structure in spider dragline silk. *Chem Commun (Camb)*, 46(36), pp. 6714-6.
- Jenkins, J.E., Sampath, S., Butler, E., Kim, J., Henning, R.W., Holland, G.P. & Yarger, J.L. (2013). Characterizing the secondary protein structure of black widow dragline silk using solid-state NMR and X-ray diffraction. *Biomacromolecules*, 14(10), pp. 3472-83.
- Jin, H.J. & Kaplan, D.L. (2003). Mechanism of silk processing in insects and spiders. *Nature*, 424(6952), pp. 1057-61.
- Jucker, M. & Walker, L.C. (2011). Pathogenic protein seeding in Alzheimer disease and other neurodegenerative disorders. *Ann Neurol*, 70(4), pp. 532-40.
- Kenney, J.M., Knight, D., Wise, M.J. & Vollrath, F. (2002). Amyloidogenic nature of spider silk. *Eur J Biochem*, 269(16), pp. 4159-63.
- Kerkam, K., Viney, C., Kaplan, D.L. & Lombardi, S. (1991). Liquid crystallinity of natural silk secretions. *Nature*, 349, pp. 596-598.
- Knight, D.P., Knight, M.M. & Vollrath, F. (2000). Beta transition and stress-induced phase separation in the spinning of spider dragline silk. *Int J Biol Macromol*, 27(3), pp. 205-10.
- Knight, D.P. & Vollrath, F. (1999). Liquid crystals and flow elongation in a spider's silk production line. *Proc. R. Soc. London*, 266, pp. 519-523.
- Knight, D.P. & Vollrath, F. (2001). Changes in element composition along the spinning duct in a *Nephila* spider. *Naturwissenschaften*, 88(4), pp. 179-82.
- Koebly, S.R., Thorpe, D., Pang, P., Chrisochoides, P., Greving, I., Vollrath, F. & Schniepp, H.C. (2015). Silk Reconstitution Disrupts Fibroin Self-Assembly. *Biomacromolecules*, 16(9), pp. 2796-804.
- Kovoor, J. (1987). IV Comparative Structure and Histochemistry of Silk-Producing Organs in Arachnids. In: *Ecophysiology*. Berlin: Springer, pp. 160-186.
- Kovoor, J. (1990). The silk-gland system in some Tetragnathinae (Araneae: Araneidae), comparative anatomy and histochemistry. *Acta Zool Fennica*, 190, pp. 215-222.
- Kronqvist, N., Otkovs, M., Chmyrov, V., Chen, G., Andersson, M., Nordling, K., Landreh, M., Sarr, M., Jornvall, H., Wennmalm, S., Widengren, J., Meng, Q., Rising, A., Otzen, D., Knight,

- S.D., Jaudzems, K. & Johansson, J. (2014). Sequential pH-driven dimerization and stabilization of the N-terminal domain enables rapid spider silk formation. *Nat Commun*, 5, p. 3254.
- Laity, P.R., Gilks, S.E. & Holland, C. (2015). Rheological behaviour of native silk feedstocks. *Polymer*, 67, pp. 28-39.
- Landreh, M., Sawaya, M.R., Hipp, M.S., Eisenberg, D.S., Wuthrich, K. & Hartl, F.U. (2016). The formation, function and regulation of amyloids: insights from structural biology. *J Intern Med*, 280(2), pp. 164-76.
- Lawrence, B.A., Vierra, C.A. & Moore, A.M. (2004). Molecular and mechanical properties of major ampullate silk of the black widow spider, *Latrodectus hesperus*. *Biomacromolecules*, 5(3), pp. 689-95.
- Lefevre, T., Boudreau, S., Cloutier, C. & Pezolet, M. (2008). Conformational and orientational transformation of silk proteins in the major ampullate gland of *Nephila clavipes* spiders. *Biomacromolecules*, 9(9), pp. 2399-407.
- Lefevre, T., Boudreau, S., Cloutier, C. & Pezolet, M. (2011a). Diversity of molecular transformations involved in the formation of spider silks. *J Mol Biol*, 405(1), pp. 238-53.
- Lefevre, T., Paquet-Mercier, F., Rioux-Dube, J.F. & Pezolet, M. (2011b). Review structure of silk by raman spectromicroscopy: from the spinning glands to the fibers. *Biopolymers*, 97(6), pp. 322-36.
- Lefevre, T. & Pezolet, M. (2012). Unexpected  $\beta$ -sheets and molecular orientation in flagelliform spider silk as revealed by Raman spectromicroscopy. *Soft Matter*, 8, pp. 6350-6357.
- LeVine, H., 3rd (1993). Thioflavine T interaction with synthetic Alzheimer's disease beta-amyloid peptides: detection of amyloid aggregation in solution. *Protein Sci*, 2(3), pp. 404-10.
- Li, S.F., McGhie, A.J. & Tang, S.L. (1994). New internal structure of spider dragline silk revealed by atomic force microscopy. *Biophys J*, 66(4), pp. 1209-12.
- Lin, S., Chen, G., Liu, X. & Meng, Q. (2016). Chimeric spider silk proteins mediated by intein result in artificial hybrid silks. *Biopolymers*, 105(7), pp. 385-92.
- Lin, Z., Deng, Q., Liu, X.Y. & Yang, D. (2013). Engineered large spider eggcase silk protein for strong artificial fibers. *Adv Mater*, 25(8), pp. 1216-20.
- Lin, Z., Huang, W., Zhang, J., Fan, J.S. & Yang, D. (2009). Solution structure of eggcase silk protein and its implications for silk fiber formation. *Proc Natl Acad Sci U S A*, 106(22), pp. 8906-11.
- Lundmark, K., Westermark, G.T., Olsen, A. & Westermark, P. (2005). Protein fibrils in nature can enhance amyloid protein A amyloidosis in mice: Cross-seeding as a disease mechanism. *Proc Natl Acad Sci U S A*, 102(17), pp. 6098-102.
- Madsen, B., Shao, Z.Z. & Vollrath, F. (1999). Variability in the mechanical properties of spider silks on three levels: interspecific, intraspecific and intraindividual. *Int J Biol Macromol*, 24(2-3), pp. 301-6.
- Magoshi, J., Magoshi, Y. & Nakamura, S. (1993). Mechanism of fiber formation of silkworm. In: *Silk Polymers* American Chemical Society, pp. 292-310.
- Meldrum, N.U. & Roughton, F.J. (1933). Carbonic anhydrase. Its preparation and properties. *J Physiol*, 80(2), pp. 113-42.

- Miao, Y., Zhang, Y., Nakagaki, K., Zhao, T., Zhao, A., Meng, Y., Nakagaki, M., Park, E.Y. & Maenaka, K. (2006). Expression of spider flagelliform silk protein in Bombyx mori cell line by a novel Bac-to-Bac/BmNPV baculovirus expression system. *Appl Microbiol Biotechnol*, 71(2), pp. 192-9.
- Miller, L.D., Putthananat, S., Eby, R.K. & Adams, W.W. (1999). Investigation of the nanofibrillar morphology in silk fibers by small angle X-ray scattering and atomic force microscopy. *Int J Biol Macromol*, 24(2-3), pp. 159-65.
- Miyake, S. & Azuma, M. (2008). Acidification of the silk gland lumen in Bombyx mori and Samia cynthia ricini and localization of a H<sup>+</sup>-translocating vacuolar-type ATPase. *J Insect Biotechnol Sericology*, 77, pp. 9-16.
- Nelson, R., Sawaya, M.R., Balbirnie, M., Madsen, A.O., Riekel, C., Grothe, R. & Eisenberg, D. (2005). Structure of the cross-beta spine of amyloid-like fibrils. *Nature*, 435(7043), pp. 773-8.
- Ohgo, K., Kawase, T., Ashida, J. & Asakura, T. (2006). Solid-state NMR analysis of a peptide (Gly-Pro-Gly-Gly-Ala)<sub>6</sub>-Gly derived from a flagelliform silk sequence of Nephila clavipes. *Biomacromolecules*, 7(4), pp. 1210-4.
- Omenetto, F.G. & Kaplan, D.L. (2010). New opportunities for an ancient material. *Science*, 329(5991), pp. 528-31.
- Otikovs, M., Chen, G., Nordling, K., Landreh, M., Meng, Q., Jornvall, H., Kronqvist, N., Rising, A., Johansson, J. & Jaudzems, K. (2015). Diversified Structural Basis of a Conserved Molecular Mechanism for pH-Dependent Dimerization in Spider Silk N-Terminal Domains. *Chembiochem*, 16(12), pp. 1720-4.
- Peakall, D.B. (1969). Synthesis of silk, mechanism and location. *Am. Zool.*, 9, pp. 71-79.
- Peng, C.A., Russo, J., Gravgaard, C., McCartney, H., Gaines, W. & Marcotte, W.R., Jr. (2016). Spider silk-like proteins derived from transgenic Nicotiana tabacum. *Transgenic Res*, 25(4), pp. 517-26.
- Perez-Rigueiro, J., Elices, M., Llorca, J. & Viney, C. (2001). Tensile Properties of Argiope trifasciata Drag Line Silk Obtained from the Spider's Web *J Appl Polym Sci*, 82, pp. 2245-2251.
- Plaza, G.R., Corsini, P., Perez-Rigueiro, J., Marsano, E., Guinea, G.V. & Elices, M. (2008). Effect of Water on Bombyx mori Regenerated Silk Fibers and Its Application in Modifying Their Mechanical Properties. *J Appl Polym Sci*, 109(3), pp. 1793-1801.
- Plaza, G.R., Guinea, G.V., Perez-Rigueiro, J. & Elices, M. (2006). Thermo-hygro-mechanical behavior of spider dragline silk: Glassy and rubbery states. *J Polym Sci Part B Polym Phys*, 44, pp. 994-999.
- Plaza, G.R., Perez-Rigueiro, J., Riekel, C., Perea, G.B., Agullo-Rueda, F., Burghammer, M., Guinea, G.V. & Elices, M. (2012). Relationship between microstructure and mechanical properties in spider silk fibers: identification of two regimes in the microstructural changes. *Soft Matter*, 8(22), pp. 6015-6026.
- Radtke, C., Allmeling, C., Waldmann, K.H., Reimers, K., Thies, K., Schenk, H.C., Hillmer, A., Guggenheim, M., Brandes, G. & Vogt, P.M. (2011). Spider silk constructs enhance axonal regeneration and remyelination in long nerve defects in sheep. *PLoS One*, 6(2), p. e16990.
- Rammensee, S., Slotta, U., Scheibel, T. & Bausch, A.R. (2008). Assembly mechanism of recombinant spider silk proteins. *Proc Natl Acad Sci U S A*, 105(18), pp. 6590-5.

- Renberg, B., Andersson-Svahn, H. & Hedhammar, M. (2014). Mimicking silk spinning in a microchip. *Sens Actuator B-Chem*, 195, pp. 404-408.
- Ridderstrale, Y. (1976). Intracellular localization of carbonic anhydrase in the frog nephron. *Acta Physiol Scand*, 98(4), pp. 465-9.
- Ridderstrale, Y. (1991). Localization of carbonic anhydrase by chemical reactions In: Dodgson, S.J., Tashian, R.E., Gros, G. & Carter, N.D. (eds) *The Carbonic Anhydrases: Cellular Physiology and Molecular Genetics*. New York: Plenum Press, pp. 133-144.
- Rising, A. (2014). Controlled assembly: a prerequisite for the use of recombinant spider silk in regenerative medicine? *Acta Biomater*, 10(4), pp. 1627-31.
- Rising, A., Hjalms, G., Engstrom, W. & Johansson, J. (2006). N-terminal nonrepetitive domain common to dragline, flagelliform, and cylindrical spider silk proteins. *Biomacromolecules*, 7(11), pp. 3120-4.
- Rising, A. & Johansson, J. (2015). Toward spinning artificial spider silk. *Nat Chem Biol*, 11(5), pp. 309-15.
- Rising, A., Widhe, M., Johansson, J. & Hedhammar, M. (2011). Spider silk proteins: recent advances in recombinant production, structure-function relationships and biomedical applications. *Cell Mol Life Sci*, 68(2), pp. 169-84.
- Rockwood, D.N., Preda, R.C., Yucel, T., Wang, X., Lovett, M.L. & Kaplan, D.L. (2011). Materials fabrication from Bombyx mori silk fibroin. *Nat Protoc*, 6(10), pp. 1612-31.
- Rousseau, M.E., Lefevre, T. & Pezolet, M. (2009). Conformation and orientation of proteins in various types of silk fibers produced by Nephila clavipes spiders. *Biomacromolecules*, 10(10), pp. 2945-53.
- Sampath, S., Isdebski, T., Jenkins, J.E., Ayon, J.V., Henning, R.W., Orgel, J.P., Antipova, O. & Yarger, J.L. (2012). X-ray diffraction study of nanocrystalline and amorphous structure within major and minor ampullate dragline spider silks. *Soft Matter*, 8(25), pp. 6713-6722.
- Sangaard, K.W., Bechsgaard, J.S., Fang, X., Duan, J., Dyrland, T.F., Gupta, V., Jiang, X., Cheng, L., Fan, D., Feng, Y., Han, L., Huang, Z., Wu, Z., Liao, L., Settepani, V., Thogersen, I.B., Vanthournout, B., Wang, T., Zhu, Y., Funch, P., Enghild, J.J., Schauser, L., Andersen, S.U., Villesen, P., Schierup, M.H., Bilde, T. & Wang, J. (2014). Spider genomes provide insight into composition and evolution of venom and silk. *Nat Commun*, 5, p. 3765.
- Schartau, W. & Leidescher, T. (1983). Composition of the hemolymph of the tarantula *Eurypelma californicum*. *J Comp Physiol*, 152, pp. 73-77.
- Scheibel, T. (2004). Spider silks: recombinant synthesis, assembly, spinning, and engineering of synthetic proteins. *Microb Cell Fact*, 3(1), p. 14.
- Schwarze, S., Zwettler, F.U., Johnson, C.M. & Neuweiler, H. (2013). The N-terminal domains of spider silk proteins assemble ultrafast and protected from charge screening. *Nat Commun*, 4, p. 2815.
- Shen, C.L. & Murphy, R.M. (1995). Solvent effects on self-assembly of beta-amyloid peptide. *Biophys J*, 69(2), pp. 640-51.
- Sipe, J.D., Benson, M.D., Buxbaum, J.N., Ikeda, S., Merlini, G., Saraiva, M.J. & Westermark, P. (2014). Nomenclature 2014: Amyloid fibril proteins and clinical classification of the amyloidosis. *Amyloid*, 21(4), pp. 221-4.

- Slotta, U., Hess, S., Spiess, K., Stromer, T., Serpell, L. & Scheibel, T. (2007). Spider silk and amyloid fibrils: a structural comparison. *Macromol Biosci*, 7(2), pp. 183-8.
- Spohner, A., Schlott, B., Vollrath, F., Unger, E., Grosse, F. & Weisshart, K. (2005a). Characterization of the protein components of *Nephila clavipes* dragline silk. *Biochemistry*, 44(12), pp. 4727-36.
- Spohner, A., Unger, E., Grosse, F. & Weisshart, K. (2004). Conserved C-termini of Spidroins are secreted by the major ampullate glands and retained in the silk thread. *Biomacromolecules*, 5(3), pp. 840-5.
- Spohner, A., Unger, E., Grosse, F. & Weisshart, K. (2005b). Differential polymerization of the two main protein components of dragline silk during fibre spinning. *Nat Mater*, 4(10), pp. 772-5.
- Spohner, A., Vater, W., Monajembashi, S., Unger, E., Grosse, F. & Weisshart, K. (2007). Composition and hierarchical organisation of a spider silk. *PLoS One*, 2(10), p. e998.
- Stadie, W.C. & O'Brien, H. (1933). The catalysis of the hydration of carbon dioxide and dehydration of carbonic acid by an enzyme isolated from red blood cells. *J Biol Chem*, 103, pp. 521-529.
- Stark, M., Grip, S., Rising, A., Hedhammar, M., Engstrom, W., Hjalms, G. & Johansson, J. (2007). Macroscopic fibers self-assembled from recombinant miniature spider silk proteins. *Biomacromolecules*, 8(5), pp. 1695-701.
- Stratakis, E. & Linzen, B. (1984). Carbonate Dehydratase (Carbonic Anhydrase) in a Spider - Association with the hemolymph lipoprotein. *Hoppe-Seyler's Zeitschrift fur physiologische Chemie*, 365(10), pp. 1187-1197.
- Suzuki, Y., Yamazaki, T., Aoki, A., Shindo, H. & Asakura, T. (2014). NMR study of the structures of repeated sequences, GAGXGA (X = S, Y, V), in *Bombyx mori* liquid silk. *Biomacromolecules*, 15(1), pp. 104-12.
- Teule, F., Addison, B., Cooper, A.R., Ayon, J., Henning, R.W., Benmore, C.J., Holland, G.P., Yarger, J.L. & Lewis, R.V. (2012). Combining flagelliform and dragline spider silk motifs to produce tunable synthetic biopolymer fibers. *Biopolymers*, 97(6), pp. 418-31.
- Teule, F., Cooper, A.R., Furin, W.A., Bittencourt, D., Rech, E.L., Brooks, A. & Lewis, R.V. (2009). A protocol for the production of recombinant spider silk-like proteins for artificial fiber spinning. *Nat Protoc*, 4(3), pp. 341-55.
- Teule, F., Furin, W.A., Cooper, A.R., Duncan, J.R. & Lewis, R.V. (2007). Modifications of spider silk sequences in an attempt to control the mechanical properties of the synthetic fibers. *J Mater Sci*, 42, pp. 8974-8985.
- Thiel, B.L., Guess, K.B. & Viney, C. (1997). Non-periodic lattice crystals in the hierarchical microstructure of spider (major ampullate) silk. *Biopolymers*, 41(7), pp. 703-19.
- Thiel, B.L., Kunkel, D.D. & Viney, C. (1994). Physical and Chemical Microstructure of Spider Dragline: A Study by Analytical Transmission Electron Microscopy. *Biopolymers*, 34, pp. 1089-1097.
- Tian, M. & Lewis, R.V. (2006). Tubuliform silk protein: A protein with unique molecular characteristics and mechanical properties in the spider silk fibroin family. *Appl Phys A Mater Sci Process*, 82, pp. 265-273.

- Tillinghast, E.K., Townley, M.A. (1994). Silk glands of araneid spiders: Selected morphological and physiological aspects. *ACS Sym Ser*, 544, pp. 29-44.
- Tjernberg, L.O., Rising, A., Johansson, J., Jaudzems, K. & Westermark, P. (2016). Transmissible amyloid. *J Intern Med*, 280(2), pp. 153-163.
- Tokareva, O., Jacobsen, M., Buehler, M., Wong, J. & Kaplan, D.L. (2014). Structure-function-property-design interplay in biopolymers: spider silk. *Acta Biomater*, 10(4), pp. 1612-26.
- van Beek, J.D., Hess, S., Vollrath, F. & Meier, B.H. (2002). The molecular structure of spider dragline silk: folding and orientation of the protein backbone. *Proc Natl Acad Sci U S A*, 99(16), pp. 10266-71.
- van Lun, M. (2013). *Structural Dynamics of Ribulose-1, 5-Biphosphate Carboxylase/Oxygenase*. Diss. Uppsala: Swedish University of Agricultural Sciences.
- Vollrath, F., Barth, P., Basedow, A., Engstrom, W. & List, H. (2002). Local tolerance to spider silks and protein polymers in vivo. *In Vivo*, 16(4), pp. 229-34.
- Vollrath, F., Holtet, T., Thogersen, H.C. & Frische, S. (1996). Structural organization of spider silk. *Proc. R. Soc. London*, 263, pp. 147-151.
- Vollrath, F. & Knight, D.P. (1999). Structure and function of the silk production pathway in the spider *Nephila edulis*. *Int J Biol Macromol*, 24(2-3), pp. 243-9.
- Vollrath, F. & Knight, D.P. (2001). Liquid crystalline spinning of spider silk. *Nature*, 410(6828), pp. 541-8.
- Vollrath, F., Knight, D.P. & Hu, X.W. (1998). Silk production in a spider involves acid bath treatment. *Proc. R. Soc. London*, 265, pp. 817-820.
- Waisbren, S.J., Geibel, J.P., Modlin, I.M. & Boron, W.F. (1994). Unusual permeability properties of gastric gland cells. *Nature*, 368(6469), pp. 332-5.
- Willcox, P.J. & Gido, S.P. (1996). Evidence of a cholesteric liquid crystalline phase in natural silk spinning processes. *Macromolecules*, 29, pp. 5106-5110.
- Winkler, S. & Kaplan, D.L. (2000). Molecular biology of spider silk. *J Biotechnol*, 74(2), pp. 85-93.
- Wright, W.W., Owen, C.S. & Vanderkooi, J.M. (1992). Penetration of analogues of H<sub>2</sub>O and CO<sub>2</sub> in proteins studied by room temperature phosphorescence of tryptophan. *Biochemistry*, 31(28), pp. 6538-44.
- Xia, X.X., Qian, Z.G., Ki, C.S., Park, Y.H., Kaplan, D.L. & Lee, S.Y. (2010). Native-sized recombinant spider silk protein produced in metabolically engineered *Escherichia coli* results in a strong fiber. *Proc Natl Acad Sci U S A*, 107(32), pp. 14059-63.
- Xu, D., Shi, X., Thompson, F., Weber, W.S., Mou, Q. & Yarger, J.L. (2015). Protein secondary structure of Green Lynx spider dragline silk investigated by solid-state NMR and X-ray diffraction. *Int J Biol Macromol*, 81, pp. 171-9.
- Xu, L., Rainey, J.K., Meng, Q. & Liu, X.Q. (2012). Recombinant minimalist spider wrapping silk proteins capable of native-like fiber formation. *PLoS One*, 7(11), p. e50227.
- Xu, M. & Lewis, R.V. (1990). Structure of a Protein Superfiber: Spider Dragline Silk. *PNAS*, 87(18), pp. 7120-7124.
- Yang, J., Barr, L.A., Fahnestock, S.R. & Liu, Z.B. (2005). High yield recombinant silk-like protein production in transgenic plants through protein targeting. *Transgenic Res*, 14(3), pp. 313-24.

- Yao, J., Ohgo, K., Sugino, R., Kishore, R. & Asakura, T. (2004). Structural analysis of Bombyx mori silk fibroin peptides with formic acid treatment using high-resolution solid-state <sup>13</sup>C NMR spectroscopy. *Biomacromolecules*, 5(5), pp. 1763-9.
- Zhang, H., Zhou, F., Jiang, X., Cao, M., Wang, S., Zou, H., Cao, Y., Xian, M. & Liu, H. (2015). Microbial production of amino acid-modified spider dragline silk protein with intensively improved mechanical properties. *Prep Biochem Biotechnol*, 46(6), pp. 552-558.
- Zhou, C.Z., Confalonieri, F., Jacquet, M., Perasso, R., Li, Z.G. & Janin, J. (2001a). Silk fibroin: structural implications of a remarkable amino acid sequence. *Proteins*, 44(2), pp. 119-22.
- Zhou, C.Z., Confalonieri, F., Medina, N., Zivanovic, Y., Esnault, C., Yang, T., Jacquet, M., Janin, J., Duguet, M., Perasso, R. & Li, Z.G. (2000). Fine organization of Bombyx mori fibroin heavy chain gene. *Nucleic Acids Res*, 28(12), pp. 2413-9.
- Zhou, L., Chen, X., Shao, Z., Huang, Y. & Knight, D.P. (2005). Effect of metallic ions on silk formation in the Mulberry silkworm, Bombyx mori. *J Phys Chem B*, 109(35), pp. 16937-45.
- Zhou, L., Chen, X., Shao, Z., Zhou, P., Knight, D.P. & Vollrath, F. (2003). Copper in the silk formation process of Bombyx mori silkworm. *FEBS Lett*, 554(3), pp. 337-41.
- Zhou, Y., Wu, S. & Conticello, V.P. (2001b). Genetically directed synthesis and spectroscopic analysis of a protein polymer derived from a flagelliform silk sequence. *Biomacromolecules*, 2(1), pp. 111-25.

## Acknowledgements

The work in this thesis was carried out at the Department of Anatomy, Physiology and Biochemistry and was generously supported by the Faculty of Veterinary Medicine and Animal Science at the Swedish University of Agricultural Sciences.

There are many I would like to thank for contributing in different ways to the work behind this thesis and I will start with expressing my sincere gratitude to my supervisors (although words just don't seem to be enough):

**Anna**, for your never-ending enthusiasm for our research and for your attention to details in anything I do, say, or write (which I have grown to love, and will miss in the future). You have been an inspiration and motivation during long hours in the lab, and you have also shown me the world during all of our trips to New York, Tokyo and Madrid. It has been a blast!

**Janne**, for sharing your passion for research in general, and spider silk in particular. You are a man of many ideas, what would we all do without you? Thanks for always looking at the bright side of every (sometimes crappy) result. I am looking forward to at least one more trip to New York, you playing guitar at my dissertation party, and Halvvättern next summer!

Many others have helped during the work with this thesis, thank you:

**Yvonne Ridderstråle**, for times at the microscope, fikas and lunches. You are a true inspiration to me both as an academic and as a strong independent woman! **Lena Holm**, for embracing that student that came into your office and started looking at tissue sections without even knowing what an epithelial cell was, for running the department in a great way, and for help with photography.

**Kerstin Nordling**, for teaching me everything I know about labwork with proteins and cloning, but most of all for always answering my numerous phone calls about ordering chemicals and supervising students. **Mitchell Chesler**, for generously inviting me to join your lab with my crazy projects during a few months. Not many would be so enthusiastic about sparing a room for twenty cages of spiders, who luckily survived hurricane Sandy!

**Thanks to all my co-authors and collaborators** - for nice papers, fruitful discussions about science, and for sharing your scientific knowledge with me. Special thanks to **Kristaps Jaudzems**, **Martins Otikovs**, and **Michael Landreh** for nice collaborations on NMR and mass spectroscopy, important parts of this thesis. **Maria Tenje**, for inviting me to join your lab and course for a few months. I learned a lot (and especially I learned how it feels to do something which you really know nothing about!). **Gustavo Plaza**, **Ana Abella** and **Xiau-Yeen Lee**, for inviting me to your lab and for performing many, many, many tensile tests on my silk fibers!

Many thanks to **past and present members of the KI spider/alzheimer group** for inspiring group meetings, christmas dinners and parties: **Jessica**, **Gefei**, and **Qiupin** (for sharing nice studies on recombinant spidroins), **Jenny** (for pushing me to buy that bike, I am forever grateful!), **Nina** (for great studies on NT and help with figures), **Médoune**, **Axel L**, **Lisa**, **Henrik**, **Axel A**, **Oihana**, **Simone**, **Jakub**, **Lorena**, **Hanna**, **Jojje**, **Erik**, **Anton**.

Many thanks to all **past and present members at the Department of Anatomy, Physiology and Biochemistry** for always cheering me on, with special thanks to **Ellinor** for pulling me down on earth and helping me realize what is important in life, I am forever grateful for your endless support! **Josefin**, **Ida** and **Anna W** for all lovely laughs and for supporting me these last few weeks, **Gugge** for helping out in the histolab, **Piotr** for helping out with all the little important things (and especially for getting me a new computer less than a week before this thesis went to print!), **Kiran** and **Liya** for keeping me company in the lab!

The Ultuna people: **Fiffi** for all the peptalks, hugs, and laughs that I desperately needed in this lonely lab (oh well, and for washing all my dishes, it was a handful...), **Emeli** for your enthusiasm for starting our own PhD seminar series, and for sharing both joy and sadness! **Sofie** for lovely lunches and fika and for talking about everything but research (well, until we both started preparing for defence) and **Oskar** for sharing the experience of writing a

thesis. Looking forward to celebrations with the both of you! **All PhD students at VHC** for nice talks during the last year at our PhD seminars, keep it up!

I would also like to thank my loving friends and family:

**Linda och Charlie** – hur hade jag klarat det senaste året utan er? Allt ifrån barnvakt, dagishämtningar, promenadsällskap, middagssällskap, hjälp att handla så vi klarade magsjukorna, till många härliga grillkvällar. Vi är er evigt tacksamma! Ni bägge, Elton, Moa och Lucas har en stor plats i mitt hjärta.

**Johanna**, tack för att du alltid finns där. Du är bäst och värd bara det bästa!

**Kina**, tack för alla långa telefonsamtal om allt annat än jobb, och för att du alltid säger vad du tycker, även när det gör ont ☺ **Lisa**, tack för din entusiasm över varje publicerad artikel, och för allt vi delat ända sedan gymnasietiden, vem kunde tro att du inte skulle bli naturvetare? **Tessan och Peter**, tack för alla vardagsmiddagar vi delat med kidsen, och för all entusiasm och omtanke ni visat för mig och mitt jobb, jag hinner snart träffas lite mer igen... **Mikael och Sandhra**, tack för härliga grillkvällar och mys med barnen!

**Anton, Sara, Elin, Vidar, Annika och Anders**, för härliga sommandagar i Lindberga, för foto-sessioner i studion, och ovärderlig hjälp med barnvakt.

**Jonas** – tack för din vetgirighet och uppmuntran. Jag önskar att du hade hunnit få den här boken, nu är jag äntligen klar!

**Mamma och pappa** - ni är bäst! Tack för att ni stöttar mig i alla mina galna infall, och för att ni alltid ställer upp med er kompetens. Alltifrån att lista ut hur man samlar hundra spindlar, till att hitta ett bra sätt att skicka hundra spindlar på posten. Extra tack för all hjälp med barnvakt de senaste månaderna, så att jag kunde skriva den här boken! **Anna, Pernilla och P-J** med familjer, tack för alla härliga galna röriga dagar i Mossebo när man inte hinner tänka på jobbet en sekund, och tack för alla härliga **syskonbarn** ni gett mig. Framtida forskare!

**Marcus** – för alla timmar du låtit mig vara på jobbet, för alla timmar du lyssnat på mig prata om jobbet, för alla timmar du hjälpt mig med jobbet, för alla timmar du låtit mig cykla, simma och springa för att koppla bort jobbet. För alla timmar tillsammans med dig, tack <3

**Jesper** – tack för att du är du – världens bästa Jeppe, som sprider glädje och kärlek och alltid har känslorna nära, jag älskar dig!